Article

Blood Leukocyte Transcriptional Modules and Differentially Expressed Genes Associated with Disease Severity and Age in COVID-19 Patients

Silvia Y. Bando [1#], **Fernanda B. Bertonha** [1#], **Sandra E. Vieira** [1#], **Danielle B. L. de Oliveira** [2,3], **Vanessa N. Chalup** [3], **Edison L. Durigon** [3], **Patricia Palmeira** [1], **Ana Cristina P. Curi** [1], **Caroline S. Faria** [4], **Leila Antonangelo** [4], **Gerhard da P. Lauterbach** [5], **Fabiane A Regalio** [6], **Roberto M. Cesar Jr** [7], **and Carlos A. Moreira-Filho**[1,*]

[1] Department of Pediatrics, Faculdade de Medicina da Universidade de São Paulo, São Paulo, SP, 05403-900, Brazil.
[2] Instituto Israelita de Ensino e Pesquisa Albert Einstein, São Paulo, SP, 01310-200, Brazil.
[3] Department of Microbiology, Laboratory of Clinical and Molecular Virology, Institute of Biomedical Sciences, Universidade de São Paulo, São Paulo, SP, 05508-040, Brazil.
[4] Laboratório de Investigação Médica (LIM03), Hospital das Clínicas, Faculdade de Medicina da Universidade de São Paulo, São Paulo, SP, 01246-903, Brazil
[5] Department of Internal Medicine, Faculdade de Medicina da Universidade de São Paulo, SP, 01246-903, Brazil.
[6] Divisão de Anestesia, Hospital das Clínicas da Faculdade de Medicina da Universidade de São Paulo, São Paulo, SP, 01246-903, Brazil.
[7] Department of Computer Science, Instituto de Matemática e Estatística da Universidade de São Paulo, SP, 05508-040, Brazil.

Silvia Y. Bando, silvia.bando@fm.usp.br, https://orcid.org/0000-0003-3794-2440
Fernanda B. Bertonha, fernanda.bernardi@fm.usp.br, https://orcid.org/0000-0002-3675-1362
Sandra E. Vieira, sandra.vieira@fm.usp.br, https://orcid.org/0000-0001-5100-8713
Danielle B. L. de Oliveira, danibruna@usp.br , https://orcid.org/0000-0002-0534-0886
Vanessa N. Chalup, vmnchalup@usp.br, https://orcid.org/0000-0002-9433-0443
Edison L. Durigon, eldurigo@usp.br, https://orcid.org/0000-0003-4898-6553
Patricia Palmeira, patricia.palmeira@hc.fm.usp.br, https://orcid.org/0000-0002-6268-8141
Ana Cristina P. Curi, anacristina.pcuri@gmail.com, https://orcid.org/0000-0002-9480-7248
Caroline S. Faria, carolmbio@gmail.com, https://orcid.org/0000-0001-5272-2169
Leila Antonangelo, l.antonangelo@hc.fm.usp.br, https://orcid.org/0000-0002-8634-5100
Gerhard da P. Lauterbach, gerhardpaz@hotmail.com, https://orcid.org/0000-0002-1448-8153
Fabiane A Regalio, fabiane.aliotti@hc.fm.usp.br
Roberto M. Cesar Jr, rmcesar@usp.br, https://orcid.org/0000-0003-2701-4288
Carlos A. Moreira-Filho, cmoreira@usp.br, https://orcid.org/0000-0003-3433-4714

* Correspondence: cmoreira@usp.br; Tel.: +55-11-97601-5087; +351-919-489-835
# SYB and FBB contributed equally to this work

Abstract: The transcriptional response of human blood leukocytes to SARS-CoV-2 infection was investigated focusing on the differences between mild and severe cases and between age subgroups. Weighted gene co-expression network analysis and comparative gene expression analysis were used. Three transcriptional modules positively associated with the traits of interest and their respective high hierarchy genes were identified. Enrichment analyses showed that the yellow module, associated with severe cases and older patients, had an overrepresentation of genes involved in inflammatory and innate immune responses, and neutrophil activation. The magenta and black modules, associated with disease severity and younger patients, contained genes related to innate immunity and inflammation and genes that regulate those responses. Subnetworks for these modules were constructed using genes enriched for innate immunity, inflammation, immunoregulation and differentially expressed genes (severe vs. mild). Their analysis evidenced that immunoregulatory functions are more activated in the modules associated with younger patients, what may help to explain the better disease course and faster recovery observed in younger COVID-19 patients.

Comparative gene expression analysis between severe and mild groups, followed by gene enrichment and normalized gene expression analyses, revelated a set of 23 potential biomarkers for COVID-19 severity, of which 13 are newly described.

Keywords: COVID-19; SARS-CoV-2; disease severity; blood leukocyte transcriptome; WGCNA; transcriptional modules; differentially expressed genes; COVID-19 transcriptional markers

1. Introduction

The study of the blood leukocyte transcriptional differences between mild and severe cases of COVID-19, as well as between age groups, brings a window of opportunity for: i) shedding light on the genomic mechanisms underlying the differences between classes of disease severity, as well as between age groups, through the comparative analysis of transcriptional modules; ii) finding, by means of differential gene expression and enrichment analyses, transcriptional biomarkers, i.e. genes, that are potential disease biomarkers and/or therapeutic targets [1,2]. Reaching of these goals is necessary for developing new therapies and better strategies for monitoring COVID-19 patients, which are demanded to avoid pressure on health systems now and in the immediate post-pandemic period (2023-2024), as shown by epidemiological studies [3].

Consequently, we decided to investigate the genomic basis of the differences between severe and mild cases of COVID-19 through a comparative study of the transcriptional responses of human leukocytes to SARS-CoV-2 infection in different age groups. We adopted a Weighted Gene Co-expression Network Analysis (WGCNA) approach [4] for identifying transcriptional modules associated with the traits of interest (severity, age) and, subsequently, we conducted differential gene expression and enrichment analyses for discovering transcriptional biomarkers, as further described in the following paragraphs.

2. Materials and Methods

2.1. Ethics Statement

This study was approved by the Research Ethics Committee of the Hospital das Clínicas da Faculdade de Medicina da Universidade de São Paulo (HC-FMUSP) under number 4.001.109. A written informed consent was obtained from all participants or from their legal guardians.

2.2. Characteristics of Participants

The participants included 121 SARS-CoV-2 PCR positive subjects recruited between May and August 2020, before the emergence of the first variant of concern in Brazil, that occurred in November 2020 [5,6] (**Table S1**). They were divided into two groups – Mild or Severe - according to the severity of illness categories described in the NIH COVID-19 Guidelines [COVID-19 Treatment Guidelines Panel. Coronavirus Disease 2019 (COVID-19) Treatment Guidelines. National Institutes of Health. Available at https://www.covid19treatmentguidelines.nih.gov/, *accessed on 12/07/21*]. The Severe group comprised 58 COVID-19 hospitalized patients requiring oxygen therapy that have been tested positive for SARS-Cov-2 by RT-qPCR and were admitted at the HC-FMUSP. The Mild group comprised 63 individuals recruited as outpatients who presented at least one of the following symptoms: fever, coryza, dyspnea, anosmia or hyposmia, ageusia or hypogeusia, wheezing in the chest, diarrhea, vomiting, body pain, headache, sore throat, or chills (**Table 1**). They were tested by nasopharyngeal swab RT-qPCR and found to be positive for SARS-Cov-2 and negative for other 15 respiratory viruses. After 14 days the clinical evolution of signs or symptoms of all these individuals was checked and the diagnosis of oligosymptomatic Covid-19 was confirmed.

Table 1. Clinical and demographic characteristics of the COVID-19 hospitalized (Severe group) and oligosymptomatic (Mild group) patients.

	Severe	Mild	*p*-value
Number of subjects	58	63	
Male	35 (60%)	25 (40%)	**0.012**
Mean age	46.3 yrs	35.3 yrs	**0.002**
Male (range)	46.4 yrs (1 mo - 81.4 yrs)	37.3 yrs (8 mo - 79.8 yrs)	0.055
Female (range)	46.1 yrs (0 mo - 75 yrs)	33.9 yrs (2.3 - 73.2 yrs)	**0.020**
Race (no. subjects)			0.268
White	37	37	
Mixed (Pardo)	21	11	
Asian	0	10	
Symptoms (no. subjects)	Yes; No;U	Yes; No;U	
Cough	47; 11	45; 11; 5	0.325
Fever	42; 16	30; 28; 5	**0.011**
Coryza	12; 46	46; 12	**0.000**
Dyspnoea	42; 12	17; 41; 5	**0.000**
Wheezing in the chest	17; 40; 1	2; 56; 5	**0.000**
Anosmia/Hyposmia	30; 23; 5	32; 24; 7	0.478
Ageusia / Hypogeusia	27; 26; 5	32; 24; 7	0.260
Headache	25; 28; 5	8; 50; 5	**0.000**
Sore throat	34; 19; 5	31; 27; 5	0.128
Diarrhea	25; 33	17; 41; 5	0.062
Vomiting	15; 41; 2	3; 55; 5	**0.000**
Body pain	21; 31; 6	14; 43; 6	0.047
Chills	33; 23; 2	0; 44; 19	**0.027**
Therapy (no. subjects)			
Oxygen	49; 4; 5	NA	
Antibiotics	42; 11; 5	9; 49; 5	
Antiviral drugs	12; 41; 5	1; 57; 5	
Corticosteroids	19; 34; 5	3; 55; 5	
Hospital stay (days)	Mean 8.5 (1 to 26)	NA	
Blood sample collection after symptom onset (range)	Median 13 days (2 - 69 d)	Median 10 days (4 - 27 d)	

U: Unknown; NA: Not applicable; mo: months; yrs: years; d: days.

2.3. Factor Analysis of Mixed Data (FAMD)

FAMD is a principal component method for analyzing a data set containing both numerical and categorical variables [7]. To perform this analysis, the Severe and Mild groups were divided into three age ranges: i) zero months to nine years; ii) 10-40 years; iii) >41 years. Numerical data was obtained from Complete Blood Count (CBC) and age, while the qualitative levels of CBC variables (low, normal, or high) according to age and sex were included as categorical variables together with sex, symptoms, and other variables of potential clinical relevance (**Table 1**). This analysis excluded missing values and comprised 64 variables and 92 individuals (**Fig. S1**). FAMD was performed using the package FactoMineR [8] in R environment [9].

2.4. Sample collection, processing, and analysis

Whole blood samples were collected from hospitalized patients (median of 13 days after first symptoms) and from oligosymptomatic individuals (median of 10 days after first symptoms). All samples were collected in EDTA-containing tubes for complete blood count analysis, white blood cell and plasma separation, and subsequent RNA extraction. Neutrophil-to-lymphocyte ratio (NLR), platelets-to-lymphocyte ratio (PLR), systemic immune-inflammation index (SII = (P × N)/L), and neutrophil-to-platelet ratio (NPR) were calculated as these hemogram-derived ratios correlate with inflammation and COVID-19 severity [10].

Nasopharyngeal and oropharyngeal samples were collected through a swab and/or a mucus specimen trap and kept under refrigeration (4ºC) up to 24 hours until cryogenic cooling and storage at -70ºC for further molecular diagnosis of SARS-CoV-2 and/or other respiratory viruses.

2.4.1. Plasma cytokine concentrations

Cytokines (IL-2, IL-4, IL-6, IL-10, IL-17, IFN-gamma, and TNF-alpha) were measured in plasma samples by flow cytometry using a BD™ Cytometric Bead Array (CBA) Human Th1/Th2/Th17 Cytokine Kit (BD Biosciences, San Jose, CA) according to the manufacturer's instructions, and the concentrations were expressed in pg/mL. Plasmatic IFN-alpha and IFN-beta were evaluated by ELISA (IFN beta and IFN alpha Duoset ELISA, R&D Systems Inc., Minneapolis, MN) and the concentrations were expressed in pg/mL.

2.4.2. Detection of respiratory viruses by RT-qPCR

Nasopharyngeal and oropharyngeal samples from oligosymptomatic individuals were obtained for RNA extraction using the NucliSens easyMag® platform fully automated (BioMerieux, Lyon, France), according to the manufacturer's instructions. RT-qPCR was employed for detecting the genetic material of SARS-CoV-2 and of 15 other respiratory viruses: influenza A virus (Inf A), influenza B virus (Inf B), seasonal coronaviruses (CoV-NL63, -229E, -HKU1, and -OC43), enterovirus (EV), parainfluenza viruses (PIV-1, -2, -3 and -4), human metapneumovirus (HMPV), rhinovirus (RV), respiratory syncytial virus (RSV), and adenovirus (AdV). A panel of validated in-house singleplex qPCR assays developed at the Centers for Disease Control and Prevention (CDC, Atlanta, GA, USA) was used according to Corman et al. [11] for SARS-CoV-2, and according to Sakthivel et al. [12] for the other viruses, using TaqMan™ assays (Applied Biosystems). For the reactions (25µL of final volume), the AgPath-IDTM™ One-Step RT Kit-PCR (Applied Biosystems) was used, and the amplification step was carried out on the ABI 7500 instrument (Applied Biosystems) under the following cycling conditions: 45°C for 10 min (1 cycle); 95°C for 10 min (1 cycle); and 95°C for 15 s, followed by 55°C for 1 min (45 cycles).

2.4.3. RNA extraction

A total of 0.5 - 1.5 mL of whole blood was used for white blood cells (WBC) RNA extraction. WBC were immediately separated by centrifugation using EL buffer (QIAamp RNA Blood Mini kit, Qiagen, Hilden, Germany). After cell separation, the WBC were collected, preserved in RNA*later* (Qiagen) and stored at 10ºC until RNA extraction. WBC were lysed with RLT buffer, and the total RNA was extracted using QIAamp® RNA Blood Mini kit (Qiagen). RNA purity analysis and quantification were performed using the NanoVue spectrophotometer (GE Heathcare Life Sciences, Marlborough, MA). RNA quality was assessed on the Agilent BioAnalyzer 2100 (Agilent, Santa Clara, USA). All RNA samples were stored at -80°C until used in hybridization experiments.

2.5. Microarray hybridization

A total of 23 RNA samples were used for gene expression analysis and grouped as Severe (n = 11) or Mild (n = 12) according to the patient's characteristics (**Table S2**). These two groups showed no significant differences regarding age, sex, and time of whole blood collection after the first day of COVID-19 symptoms. The Severe group was further

divided into subgroups A and B, where A included the samples from adolescents and younger adults (age ranging from 11 to 38 years; n = 5) and B included the samples from older adults (age ranging from 41 to 62 years; n = 6). Similarly, the Mild group was divided in subgroups C and D, where C included the samples from adolescents and younger adults (age ranging from 10 to 37 years; n = 7) and D included the samples from older adults (age ranging from 41 to 64 years; n = 5). The patients between zero and nine years (Severe and Mild groups) were not included due to insufficient RNA quality.

To determine gene expression profiles, 4×44K DNA microarrays (Whole Human Genome Microarray Kit, Agilent Technologies, cat no. G4845A) were used. The procedures for hybridization using the fluorescent dye Cy3 followed the manufacturer's protocols (One-Color Microarray-Based Gene Expression Analysis—Quick Amp Labeling). The images were captured by the reader Agilent Bundle according to the parameters recommended for bioarrays and extracted by Agilent Feature Extraction software version 11.5.1.1 (https://www.agilent.com/). Spots with two or more flags (low intensity, saturation, controls, etc.) were considered as NA, that is, without valid expression value. All microarray raw data have been deposited in GEO public database (http://www.ncbi.nlm.nih.gov/geo), a MIAME compliant database, under accession number GSE193022.

2.6. Gene expression analysis

An in-house algorithm in R environment [9] was used for excluding transcripts presenting one or more missing values (NAs) per group and for converting gene expression values to log base 2. Through this procedure we obtained two gene expression data matrices: i) one for gene co-expression network (GCN) analysis, and ii) another for differential gene expression (DEG) analysis. The GCN matrix had 6,375 Gene Ontology (GO) annotated genes after excluding all NAs. The DEG matrix had 15,248 GO annotated genes, including NAs and with a minimum of four valid gene expression values per group. Data normalization was performed using limma package [13,14] in R environment [9]. The differential gene expression analyses were conducted in three comparisons separately: i) Severe *vs*. Mild ii) A *vs*. B; iii) C *vs*. D.

2.7. Weighted Gene Co-expression Network Analysis (WGCNA)

The network was constructed using the WGCNA package [15] (version 1.69–81; https://horvath.genetics.ucla.edu/html/CoexpressionNetwork/Rpackages/WGCNA/) in R environment [9]. Pearson's correlation coefficient was used for obtaining gene co-expression similarity measures and for the subsequent construction of an adjacency matrix using soft power and topological overlap matrix (TOM). Soft thresholding process transforms the correlation matrix to mimic the scale-free topology. TOM is used to filter weak connections during network construction. Module identification is based on TOM and on average linkage hierarchical clustering. The soft power β = 20 (R^2 = 0.9160) was chosen using the scale-free topology criterion (**Fig. S2**). Finally, Dynamic Tree Cut algorithm [4] was used for dendrogram's branch selection. The module eigengene (ME) is defined as the first principal component of a given module, which can be considered a representative of the gene expression profiles in a module. Module Membership (MM), also known as eigengene-based connectivity (*k*ME), is defined as the correlation of each gene expression profile with the module eigengene of a given module.

2.7.1. Module-trait association

Module-trait association analysis was accomplished using the WGCNA package [15] in R environment [9]. For this analysis we considered as specific traits: severity group, age subgroup, and clinical laboratory characteristics]. Subsequently, the gene significance (GS), i.e., a value for the correlation between specific traits and gene expression profiles [15] was obtained. The mean GS value for a particular module is considered as a measure of module significance (MS). Modules presenting a significant *p*-value ($p < 0.05$) and a positive trait correlation were selected for functional analysis.

2.7.2. Node categorization

All genes belonging to a given module were designated here as ME genes (for module eigengene gene). The modules significantly correlated to specific traits (age group, clinical, and laboratory data) were further evaluated for identifying relevant hub genes, i.e., the highly connected genes, here termed high-hierarchy (HH) genes, that hold the transcriptional network together and are also associated to specific cellular processes or link different biological processes [16,17]. Thus, connectivity measures were used for the hierarchical categorization of hub genes, considering connectivity values related to the network (overall connectivity) and to the module (intramodular connectivity for each gene based on its Pearson's correlation with all other genes in the module).

Intramodular node connectivity was calculated considering: (i) kTotal, the whole network connectivity of each gene; (ii) kWithin, gene connections with other genes in the same module [15]. Genes presenting high kTotal and kWithin are classified as high hubs (Hhubs), genes presenting high kTotal but low kWithin are called eHubs, and genes presenting high kWithin but low kTotal are the iHubs. The iHubs connect most of the genes in a transcriptional module, whereas the eHubs connect different transcriptional modules, and the Hhubs hold the transcriptional modules and the network together [17,18]. The top 10 genes presenting the highest kTotal and/or kWithin values were selected as HH genes. All gene values were plotted in a kTotal (x-axis) *vs.* kWithin (y-axis) graph. Additionally, the expression profile was assessed for the selected hubs through GS values, ie., the GS of the nth gene is the correlation measure between the nth gene expression and the specific trait. Positive or negative GS values mean that the nth gene is hyper- or hypo-expressed for the specific trait. Only GS values with $p < 0.01$ were considered significant for the trait.

2.8. Enrichment analyses

WGCNA modular gene set enrichment analyses for Gene Ontology Biological Process (GO BP), KEGG pathways, and Reactome pathways were accomplished by using the Enrichr online web-based tool [19]. The terms presenting adjusted p-value < 0.05 for the modules or p-value < 0.05 for the hub genes, were considered significantly enriched. The same enrichment analysis strategy was applied for all hub genes and DE genes.

2.9. Statistical analysis

Significance analysis for microarray (SAM) using MeV software (version 4.9.0) was used for differential gene expression analyses. T-test was used for statistical analysis of the clinic-demographical data and differentially expressed genes employed in GraphPad Prism (version 8). The relative expression of the differentially expressed genes (DEGs) was normalized with the endogenous reference gene *GUSB* for statistical analysis (**Table S2**). The FAMD analysis was performed as described in section 2.3.

2.10. Gene co-expression network (GCN)

The GCNs were constructed by using Pearson's correlation. Data analysis and visualization were accomplished through Cytoscape [20] version 3.9.0.

3. Results

3.1. Patient demographic and clinical characteristics

The clinical and demographic characteristics of the severe (hospitalized) and mild (oligosymptomatic) COVID-19 patients are shown in **Table 1.** The average age for the Severe and Mild groups was significantly different: 46.3 years and 35.3 years, respectively ($p = 0.002$). There was a predominance of males ($p = 0.012$) in the Severe group (60%) as compared to the Mild group (40%). In the Severe group more patients presented fever, dyspnea, wheezing in the chest, and vomiting, while more oligosymptomatic individuals presented coryza and headache (**Table 1**). A significantly higher number of patients in the

Severe group presented at least one comorbidity. In a decreasing order of frequency: systemic arterial hypertension, diabetes mellitus, obesity, cardiopathy, pneumopathy, and nephropathy (**Fig. 1**).
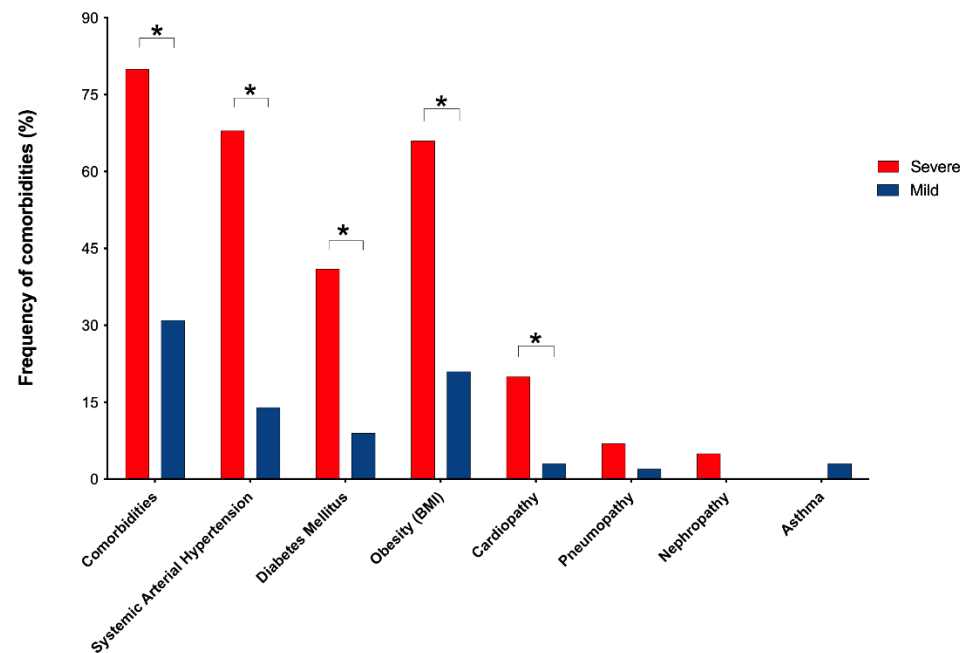

Figure 1. Frequency of comorbidities in COVID-19 patients. Frequency of comorbidities among the patients (n = 121) with confirmed SARS-CoV-2 infection. Severe and mild phenotypes are depicted by red and blue bars, respectively. Differences were tested using one-tailed Mann-Whitney t test (*p < 0.01). *Stands for comorbidities significantly correlated with COVID-19 patients with a severe outcome.

The hemogram results were interpreted as normal, high, or low, based on reference values for age and sex (**Table S4**). The comparative analysis between the Severe and Mild groups showed that more individuals in the Severe group presented high values for segmented neutrophils and low values for erythrocytes, hematocrit, hemoglobin, lymphocytes, and immature neutrophils (**Fig. 2**). Severe patients had significantly elevated values for all hemogram-derived ratios when compared to Mild (i.e., oligosymptomatic) patients (**Table 2**), and higher values were found for PLR and SII parameters in the subgroups B and D (patients over 41 years of age)**.** Additionally, the individuals in the Severe group expressed higher levels of IL-6 and IL-10 when compared with the Mild group. The cytokines IL-4, IL-2, and IFN-γ, were also elevated in these individuals (**Fig. 3**).
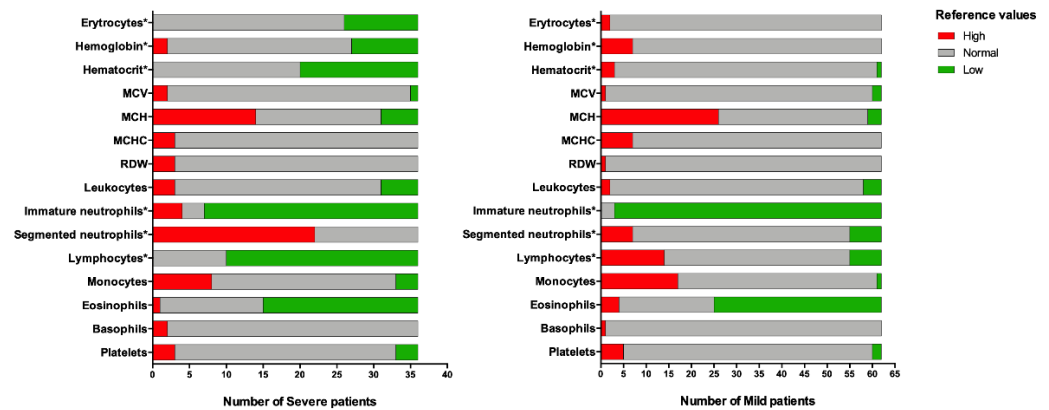
Figure 2. Hematological findings in COVID-19 patients. Hematological findings for both severe (left panel) and mild (right panel) phenotypes. Colored bars indicate the number of patients presenting high blood count values (in red), low blood count values (in green), and normal blood count reference values (in grey). *Significant correlation with severity was found for high values of immature and segmented neutrophils, and low levels of erythrocytes, hemoglobin, hematocrit, and lymphocytes ($p < 0.005$). MCV: Mean Corpuscular Volume, MCH: Mean Corpuscular Hemoglobin, MCHC: Mean Corpuscular Hemoglobin Concentration, RDW: Red cell Distribution Width.

Table 2. Comparative analyses of the hemogram-derived ratios between Severe and Mild groups.

Hemogram-derived ratio	Severe (mean, STD)		Mild (mean, STD)		*p*-value (Mann-Whitney)
	A (10-40yrs)	B (41-80yrs)	C (10-40yrs)	D (41-80yrs)	
NLR	**4.99 (5.64)**		**1.68 (1.86)**		**< 0.0001**
Ratio value (mean, STD)	3.35 (2.01)	5.95 (6.67)	1.38 (0.82)	2.42 (2.88)	
p-value (Mann-Whitney)	NS		0.009		
NPR	**2.04 (1.14)**		**1.25 (0.62)**		**0.0002**
Ratio value (mean, STD)	2.00 (1.20)	2.20 (1.10)	1.20 (0.53)	1.50 (0.71)	
p-value (Mann-Whitney)	NS		NS		
PLR	**0.21 (0.33)**		**0.09 (0.07)**		**< 0.0001**
Ratio value (mean, STD)	0.11 (0.03)	0.27 (0.40)	0.08 (0.05)	0.11 (0.09)	
p-value (Mann-Whitney)	0.0055		0.0417		
SII	**16.86 (31.00)**		**4.89 (5.75)**		**< 0.0001**
Ratio value (mean, STD)	7.10 (2.90)	22.00 (38.00)	4.10 (3.80)	6.90 (8.20)	
p-value (Mann-Whitney)	0.0191		0.0166		

NLR: neutrophil-lymphocyte ratio; NPR: neutrophil-to-platelet ratio; PLR: Platelet-to-lymphocyte ratio; SII: systemic immune-inflammation index; STD: Standard Deviation; NS: Not significant; yrs: years
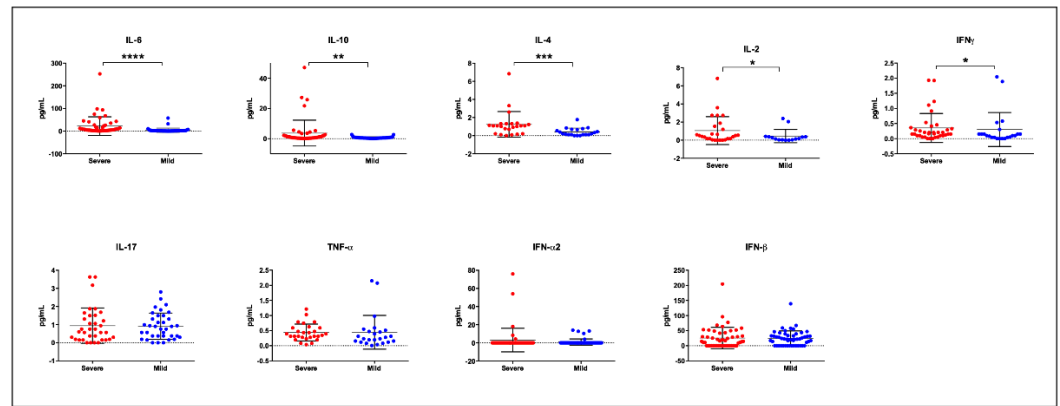
Figure 3. Plasmatic cytokine levels. The dot plots show the comparisons of plasmatic cytokine (IL-2, IL-4, IL-6, IL-10, IL-17, TNF-α, IFN-α2, and IFN-β) concentrations (pg/mL) between severe and mild cases. The data are presented as the mean with SD. Differences were tested using one-tailed Mann-Whitney t test (**** $p < 0.00001$; *** $p < 0.0001$; ** $p < 0.001$; * $p < 0.01$).

FAMD analysis for clinical characteristics yielded six dimensional clusters for patients aged 0-9, 10-40 and over 40 years, in the Severe and Mild groups (**Fig.4**). All patients selected for transcriptomics studies are contained in four dimensional clusters: 10-40 and over 40 years for both Severe and Mild groups.
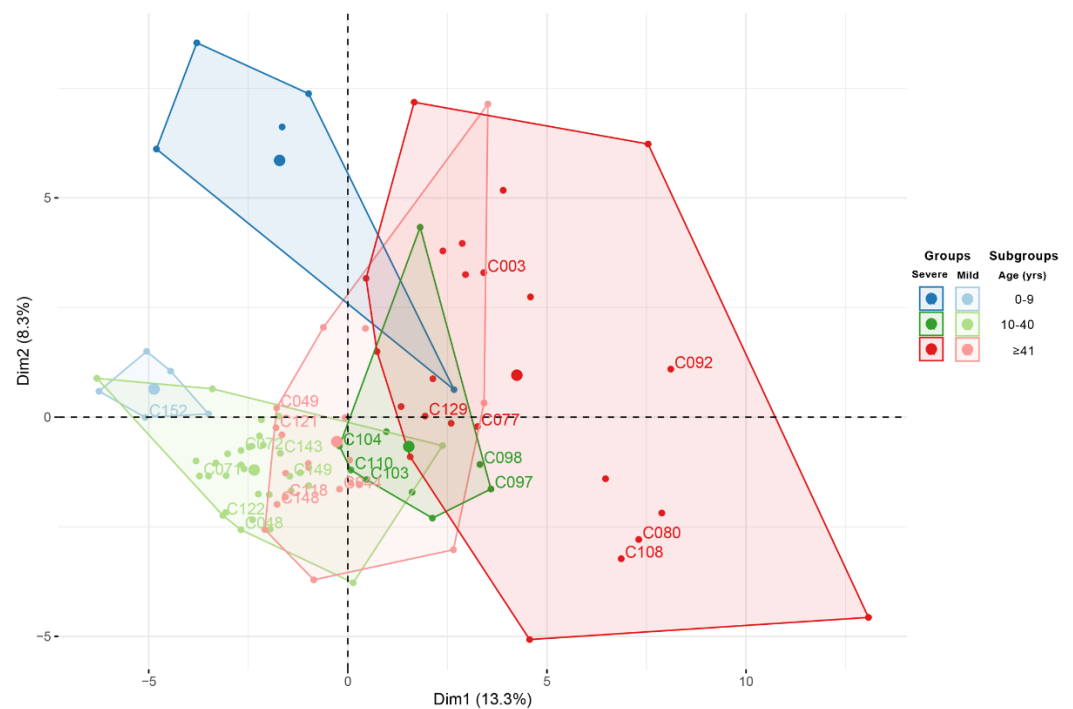

Figure 4. Exploratory multivariate analysis. Factor Analysis of Mixed Data (FAMD) with grouping variables identified four dissimilar groups: the two main groups (severe and mild), and the two age-related subgroups (10-40 years old; 41-85 years old).

3.2. WGCNA and Module-Trait Correlation Analysis

The normalized gene expression data of 6,375 GO annotated genes were used for network construction and module identification by WGCNA. Nine transcriptional modules were identified. Module sizes ranged from 147 genes in the magenta module to 891 genes in the turquoise module (**Fig. S3**). The hierarchical clustering dendrogram of module-eigengenes revealed two meta-modules. In the meta-module I the transcriptional modules are correlated with severe phenotypes, whereas the in the meta-module II the correlation is with mild phenotypes (**Fig. 5A**). The module-trait correlation analysis identified three transcriptional modules with at least one significant correlation ($p < 0.05$) with

disease severity (Severe; Mild), age subgroups (A; B), or CBC traits (**Fig. 5B** and **Fig. S3**). The yellow module is positively correlated with the Severe group, with subgroup B (old and severe), with high level of segmented neutrophils, and with low level of lymphocytes. The magenta module is positively correlated with the Severe group, subgroup A (young and severe), and with high level of segmented neutrophils. The black module is positively correlated with subgroup A and with high level of segmented neutrophils (**Fig. 5B**).

A

B

	Modules		
Number of genes	479	147	342
Traits	**Yellow**	**Magenta**	**Black**
Severe group	0.70 (3e-4)	0.44 (0.04)	
Subgroup A		0.47 (0.03)	0.48 (0.02)
Subgroup B	0.46 (0.03)		
H-SN	0.72 (1e-4)	0.46 (0.03)	0.48 (0.02)
L-Lymphs	0.51 (0.02)		
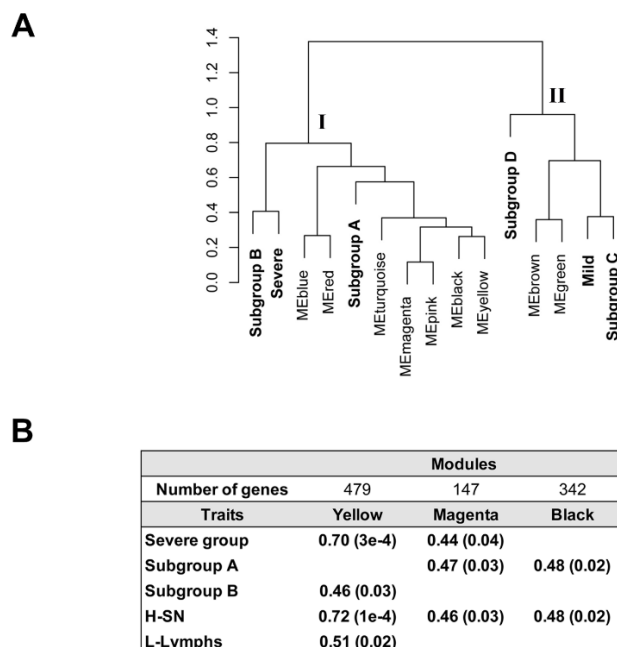
Figure 5. Module-trait relationships. Eigengene dendrogram shows the correlation between modules and traits (severity and age) (**A**). Significant module-trait correlations with severity groups, age subgroups, and neutrophil and lymphocyte levels are depicted in (**B**). The traits of interest appear in the rows and the modules appear in the columns. The numbers stand for the correlation coefficients between the module and a specific trait, with the p-values between parentheses. Only the positive module-trait correlations are shown ($p < 0.05$). H-SN: high level of segmented neutrophils, L-Lymphs: low level of lymphocytes.

We also performed a functional characterization of these three transcriptional modules and identified their high hierarchy (HH) genes. Transcriptional modules often represent biological processes that can be phenotype-specific [18]. The functional enrichment among the genes within a module is widely used for disclosing its biological meaning [18]. Here, KEGG, Reactome and GO BP databases were used for the gene enrichment analysis and consequent functional characterization of the three transcriptional modules significantly correlated with severity groups and/or age subgroups (**Fig. 5B**). The terms presenting adjusted p-value < 0.05 were considered significantly overrepresented in those modules (**Figs. 6-8**) and the lists of genes and terms for each module are presented in **Tables S5-S7.**
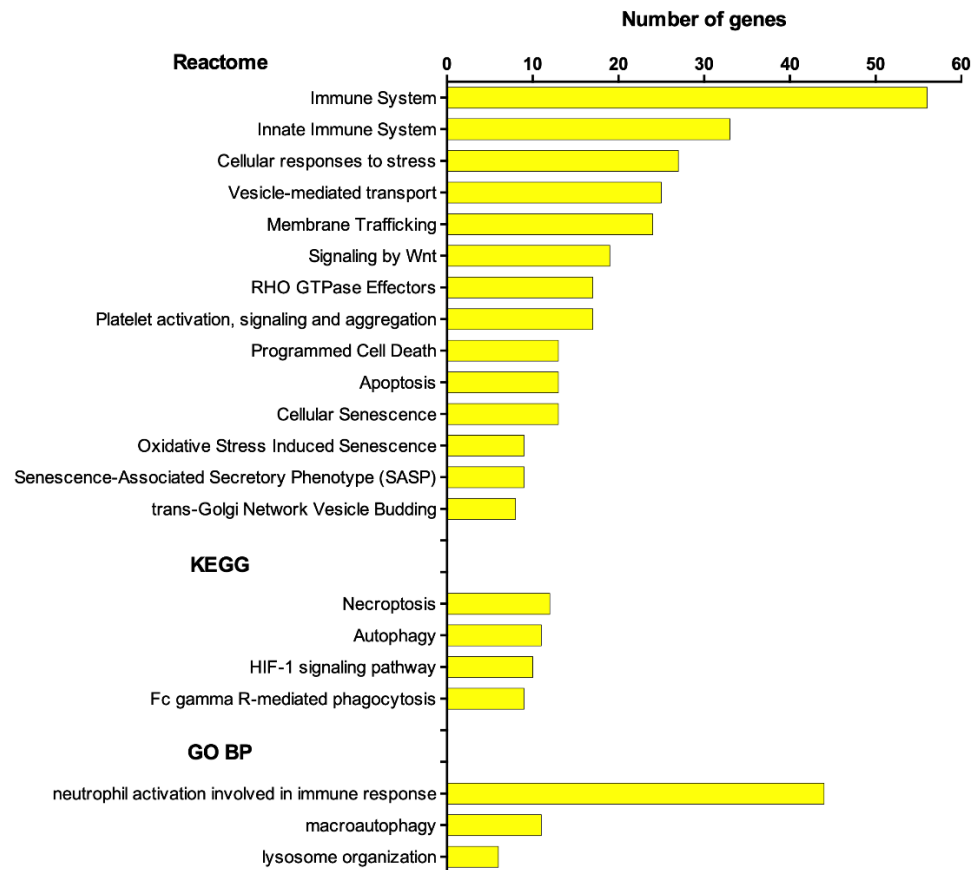
Figure 6. Histogram of enriched Reactome, KEGG pathways, and GO BP terms for the yellow module. The terms with adjusted $p < 0.05$ were considered significant.
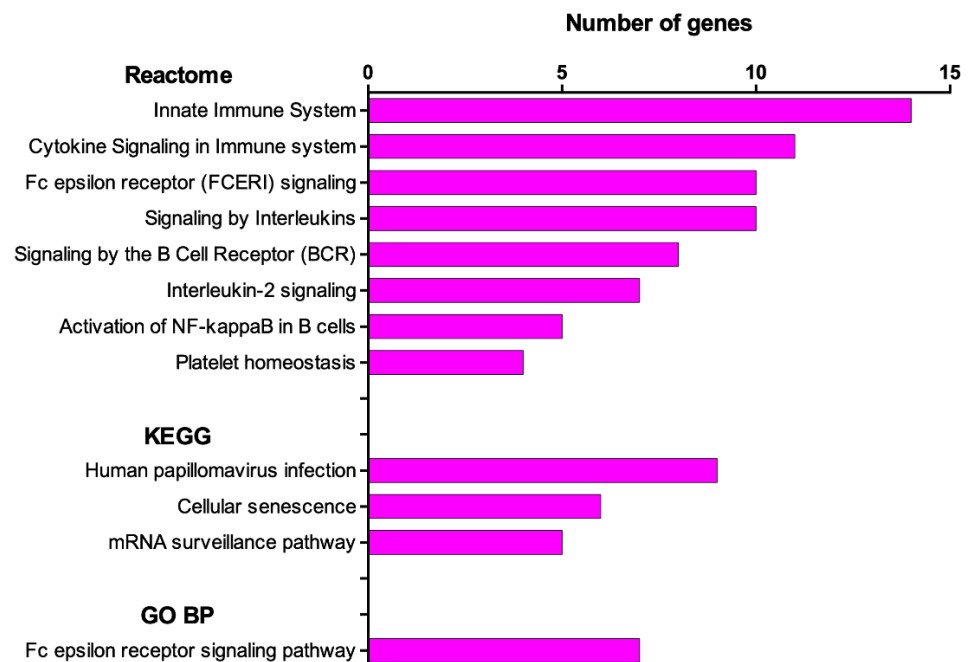

Figure 7. Histogram of enriched Reactome, KEGG pathways, and GO BP terms for the magenta module. The terms with adjusted $p < 0.05$ were considered significant.
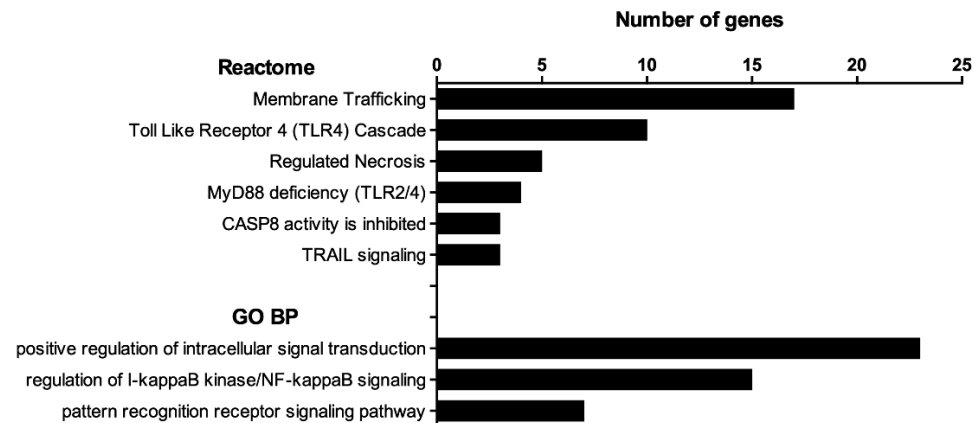
Figure 8. Histogram of enriched Reactome and GO BP terms for the black module. The terms with adjusted $p < 0.05$ were considered significant.

Through the calculation of intramodular node connectivity, a total of 40 HH genes were found in the three modules significantly related to traits, which were subsequently classified into three hierarchical categories: i) iHubs, which connect most of the genes in a transcriptional module; ii) eHubs, that connect different transcriptional modules; iii) Hhubs, which hold the transcriptional module and the network together (**Table 3** and **Fig. S4**).

Table 3. High hierarchy genes (Hhubs, iHubs, and eHubs) of the modules significantly and positively correlated with at least one trait (Severe group, subgroups A and B, H-SN, and L-Lymphs). Each HH gene is identified by its hierarchical categorization, GO biological process or molecular function, and KEGG Pathways-related terms (in bold letters). Only positive (i.e., hyper-expressed) or negative (i.e., hypo-expressed) significant GS values for a specific trait (p < 0.01) are shown.

Yellow module			GS Values	
Gene	Category	GO Databases: Biological Process (BP), Molecular Function (MF); KEGG Pathways	Severe	H-SN
TMEM59	Hhub	autophagy	0.59	0.62
DECR1		fatty acid beta-oxidation		
ATP6V1E1		regulation of macroautophagy; **mTOR signaling pathway**		
PRDX3		cellular response to oxidative stress	0.59	0.59
SDHB		**oxidative phosphorylation**		
METTL6		tRNA methylation		
EIF4A3	eHub	mRNA splicing, via spliceosome	0.59	
COPS5		ubiquitination; regulation of stress-activated MAPK cascade		
PAPD4 (TENT2)		histone mRNA catabolic process		0.62
TXNDC12		endoplasmic reticulum stress-induced intrinsic apoptosis		
SNAPIN	iHub	autophagosome maturation	0.60	
MBD2		methylation-dependent chromatin silencing		
SPTLC1		macroautophagy; **sphingolipid metabolism**	0.66	0.70
C1GALT1C1		**mucin type O-glycan biosynthesis**	0.61	0.62
Black module			**GS Value**	
Gene	Category	GO Databases: Biological Process (BP), Molecular Function (MF); KEGG Pathways		H-SN
EVX1	Hhub	transcription by RNA polymerase II; transcriptional repressor during embryogenesis		
SHISA4		protein binding		

Gene	Category	GO Databases	GS
CYGB		response to oxidative stress	
LOC113230 (MISP3)		MISP family member 3	
FHL1		potassium ion transport; negative regulation of cell growth; **JAK-STAT signaling pathway**	
CACNA1C		**calcium signaling pathway**	
HBZ	eHub	zeta-globin	-0.58
PTMA		negative regulation of apoptotic process; transcription	
RAC1		**Rap1 signaling pathway; Ras signaling pathway**	
FOXP4	iHub	transcription	
DPEP3		proteolysis	
UCP3		mitochondrial membrane transport	
PYY2		pseudogene	
Magenta module			
Gene	**Category**	**GO Databases: Biological Process (BP), Molecular Function (MF); KEGG Pathways**	
DHX15	Hhub	RNA splicing	
RNF114		ubiquitination	
DHX29		RNA helicase, member of the DEAH subfamily (DEAD box family)	
KIAA0196 (WASHC5)		endosome fission	
CNOT8		transcription; **RNA degradation**	
HTR3A		ion transmembrane transport; **serotonergic synapse**	
PPP2CA		**TGF-beta signaling pathway; hippo signaling pathway; PI3K-Akt signaling pathway**	
PSMD10	eHub	negative regulation of NF-kappaB transcription factor activity	
SYNGR4		integral component of membrane	
JTB		protein kinase binding	
ARL6IP1	iHub	ER tubular network formation	
SLBP		histone pre-mRNA stem-loop binding	
RASSF5		apoptotic process; **cellular senescence; Rap1 and Ras signaling pathway**	

H-SN: high percentage of segmented neutrophils in the hemogram; GS: Gene Significance

3.2.1. Yellow module

The enrichment analyses for this module, that belongs to the meta-module I (severe phenotypes, **Fig. 5A**) appear in **Figure 6** and **Table S5**. The KEGG analysis showed an overrepresentation of genes involved in inflammation and immune response, namely in necroptosis, autophagy, and Fc gamma R-mediated phagocytosis. Noteworthy, it is also enriched for genes involved in the HIF-1 signaling pathway, that are hyper-expressed in the peripheral blood mononuclear cells (PBMC) of COVID-19 patients [21] and aggravate inflammatory responses [22]. The genes over-represented in the Reactome were mostly related with immune system, innate immunity, inflammation, cell death, cellular senescence, and neutrophil effector pathways. Regarding the GO BP analysis, the most represented category is related to neutrophil activation (44 genes), what is quite expectable due to the role of neutrophils in restricting viral replication and diffusion [23]. The other well represented categories in GO BP analysis encompass genes involved in macroautophagy and lysosome organization. Therefore, the most represented cellular processes and functional pathways in the yellow module mainly reflect the inflammatory and innate immune responses against SARS-CoV-2 [24].

The yellow module harbors 14 HH genes (**Table 3**). The Hhubs *TMEM59* [25] and *ATP6V1E1* [26], and the iHubs *SPTLC1* [27] and *SNAPIN* [28] are autophagy-related genes, the latter being critical for autophagosome maturation in macrophages. Two Hhubs - *PRDX3* [29] and *SDHB* [30] - are involved in the protection against oxidative stress. The eHub *TXNDC12* (alias *ERP16*) takes part in the cellular defense against prolonged ER stress [31]. A decrease in ER-stress was shown to occur in a stage-specific manner during neutrophil and macrophage differentiations [32]. The iHub *C1GALT1C1* codes for a molecular chaperone (Cosmc) that plays a crucial role TRAIL-induced apoptosis [33]. A well-balanced IFN/TRAIL response is necessary for overcoming viral infections [34]. Finally, it is important to mention that in this module seven HH genes also have high GS values. Four of these genes - *TMEM59, PRDX3, SPTLC1*, and *C1GALT1C1* – are positively correlated with the Severe group and with high level of segmented neutrophils. Two other genes - *EIF4A3*, a modulator of the non-sense mediated mRNA decay pathway [35] and *SNAPIN* - are positively correlated with the Severe group. *TENT2* (alias *PAPD4*), a gene involved in miRNA processing [36], is positively correlated with high level of segmented neutrophils. Taken together, the gene enrichment analyses and the functional characterization of the HH genes for the yellow module fairly agree with the positive correlation of this module with COVID-19 severe cases, with subgroup B (aged and severe patients), and with high number of segmented neutrophils and lymphopenia (i.e., elevated NLR and SII; **Table 2**), two hallmarks of COVID-19 severity [37].

3.2.2. Magenta module

The enrichment analyses are shown in **Fig. 7** and **Table S6**. The Reactome enrichment results show an overrepresentation of pathways related with immune response and inflammation, such as innate immune system, cytokine signaling, Fc epsilon receptor signaling, signaling by interleukins, signaling by the B cell receptor, interleukin-2 signaling, activation of NF-κB in B cells, TCR signaling, and platelet homeostasis. The GO BP enrichment yielded only one term, the Fc epsilon receptor signaling pathway. Three pathways were found through KEGG enrichment: cellular senescence, human papilloma virus infection, and mRNA surveillance pathway. Hence, the functional enrichment for the magenta module reveals a predominance of pathways related with innate and adaptive immune responses and inflammation. Moreover, the Fc epsilon receptor signaling pathway indicates the involvement of basophils and, indeed, it was recently shown that these cells play an active role in the immunity against SARS-CoV-2 [38].

The magenta module has 13 HH genes (**Table 3**) and most of them act on the modulation of the innate and adaptive antiviral immune responses. The Hhub *PPP2CA* codifies protein phosphatase 2A, an important regulator of inflammatory signaling [39]. The Hhub *RNF114* codes for a RING-type zinc-finger protein that modulates NF-κB activity and T-cell activation [40]. The Hhub *HTR3A* encodes the subunit A of the 5-HT3 receptor of serotonin, found in monocytes, B and T cells and probably involved in their recruitment to sites of inflammation [41,42]. Decreased serum levels of serotonin were found in severe cases of COVID-19, whereas in the mild cases the serotonin levels were close to those found in control individuals [43]. The Hhubs *DHX15* [44] and *DHX29* [45] code for two DEAH-box helicases that are key sensors for antiviral defense against RNA virus infection. The Hhub *WASHC5* codes for strumpellin, a protein involved in endosomal fission [46] that was shown to interact directly with SARS-CoV-2 [47]. The Hhub *CNOT8* encodes the CNOT8 catalytic subunit of the CCR4-NOT complex, which is required for selective mRNA degradation (mRNA surveillance) and for preventing excessive inflammatory responses [48]. The eHub *PSMD10* codes for gankyrin and promotes autophagy [49], a crucial innate immune response against infection. The eHub *SYNGR4* codes for the integral membrane component synaptogyrin and promotes endosome recycling [50] that is essential for cytokine release by neutrophils [51]. The eHub *JTB* (alias *PAR*) acts on the regulation of mitochondrial function [52] and the low expression of mtDNA in the immune system cells of COVID-19 patients was recently reported [53]. Lastly, there are three iHubs: *SLBP*, which encodes a TNF-induced stem-loop binding protein that regulates histone

metabolism, inflammation, and viral replication [54]. *RASSF5* (alias *NORE1A*), an apoptosis inducer and senescence effector [55]; and *ARL6IP1*, that codes for an ER-shaping protein/ involved in the fine control of ER organization [56].

The magenta module belongs to the meta-module I (**Fig. 5A**) and is positively correlated with the Severe group, with the subgroup A (young and severe patients), and with high level of segmented neutrophils. These correlations fit in well with the enrichment terms and the functional profile of the HH genes found for this module. The pathway analyses reveal a preponderance of terms related to innate and inflammatory immune responses, reflecting the module's correlation with disease severity traits. On the other hand, several HH genes seem to play a modulatory role in immune and inflammatory responses, thus preventing the progression to critical illness.

3.2.3. Black module

The enriched pathways in the black module (**Fig. 8** and **Table S7**), that belongs to meta-module I (**Fig. 5A**) and is positively correlated with the subgroup A (young and severe patients) and with high level of segmented neutrophils (**Fig. 5B**), reflect some of the main mechanisms involved in the innate immune and inflammatory responses to SARS-CoV-2. The Reactome pathways TLR/4, MyD88/TLR2, CASP8, TRAIL signaling, and necrosis are mechanistically related and take part in the recognition of viral proteins, inflammatory responses, and cell death [57]. Interestingly, the increased expression of TLRs and MyD88 were found to be positively correlated with COVID-19 severity [58]. The GO BP pathways are related to intracellular signal transduction, pattern recognition receptor signaling (including TLRs, see **Table S7**) and to the I-kappaB Kinase/NF-kappaB signaling, a master regulator of inflammatory and immune responses [59,60].

This module has 14 HH genes (**Table 3**) of which five are directly related to immune response regulation. The Hhub *CACNA1C* codes for the alpha-1 subunit of CaV1.2 calcium channel and is involved in the regulation of human Th2-lymphocyte functions [61]. The eHub *RAC1* codifies a Rho GTPase that triggers NFκB activation [62]. The eHub *PTMA* encodes prothymosin-alpha, an alarmin involved in cell proliferation, apoptosis, and immune regulation and whose expression in CD8 T memory stem cells is increased in COVID-19 [63]. The iHub *FOXP4* codifies a transcription factor required for T cell recall response to pathogens [64]. The iHub *UCP3* codes for an uncoupling protein (UC) involved in the maintenance of Th17/Treg cell balance [65], which is skewed towards Th17 in COVID-19 [66].

The other HH genes in the black module are involved in different biological functions, some of them possibly related to modulatory mechanisms acting on inflammatory and immune responses. The Hhub *CGYB* codes for cytoglobin, a protein that protects cells against oxidative stress [67]. The Hhub *FHL1* encodes a four-and-a-half-LIM-domain protein involved in gene transcription regulation, cytoarchitecture, cell proliferation, and signal transduction [68]. Interestingly, FHL1 inhibits the vascular endothelial growth factor (VEGF) expression [69] and elevated serum levels of VEGF were positively correlated with disease severity in COVID-19 [70]. The Hhub *MISP3* codes for a protein involved in spindle orientation and mitotic progression [71]. The Hhub *EVX1* encodes a transcriptional repressor [72] and the Hhub *SHISA4* codes for a transmembrane adaptor protein [73]. The iHub *DPEP3* encodes dipeptidase 3, involved in the hydrolytic metabolism of dipeptides, and the iHub *PYY2* is a pseudogene coding for peptide YY2. Finally, the eHub *HBZ* codes for zeta hemoglobin and HBZ expression may be interpreted as evidence for circulating erythroid precursors in hospitalized (requiring oxygen) patients [74-76], being negatively correlated with hemoglobin levels. *HBZ* has a negative GS value for the H-SN trait (**Table 3**).

3.3. *Differential gene expression analyses*

Two comparative gene expression analyses (SAM) were conducted: i) Severe *vs*. Mild groups; ii) A *vs*. B subgroups. In the Severe *vs*. Mild comparison 50 differentially expressed genes (DEGs) were found, of which 49 were hyper-expressed in the Severe group, with

fold-changes ranging between 8.8 and 2.0. The comparative analysis between the sub-groups A and B yielded only two DEGs, one hyper-expressed in A and another in B, with fold-changes of 3.0 and 3.50, respectively.

Subsequent enrichment analysis for the DEG set of the Severe group was accomplished using GO BP and KEGG pathways databases. The significant terms (*p*-value < 0.05) overrepresented in these two DEGs sets are listed in **Tables S8**. The KEGG enrichment analysis for the Severe group showed DEGs mainly related with p53 and Hippo signaling, neutrophil extracellular trap formation, and cellular senescence, whereas the GO BP enrichment analysis showed several terms related with neutrophil activation, innate immune response, and inflammation (**Fig. 9** and **Table S8**).
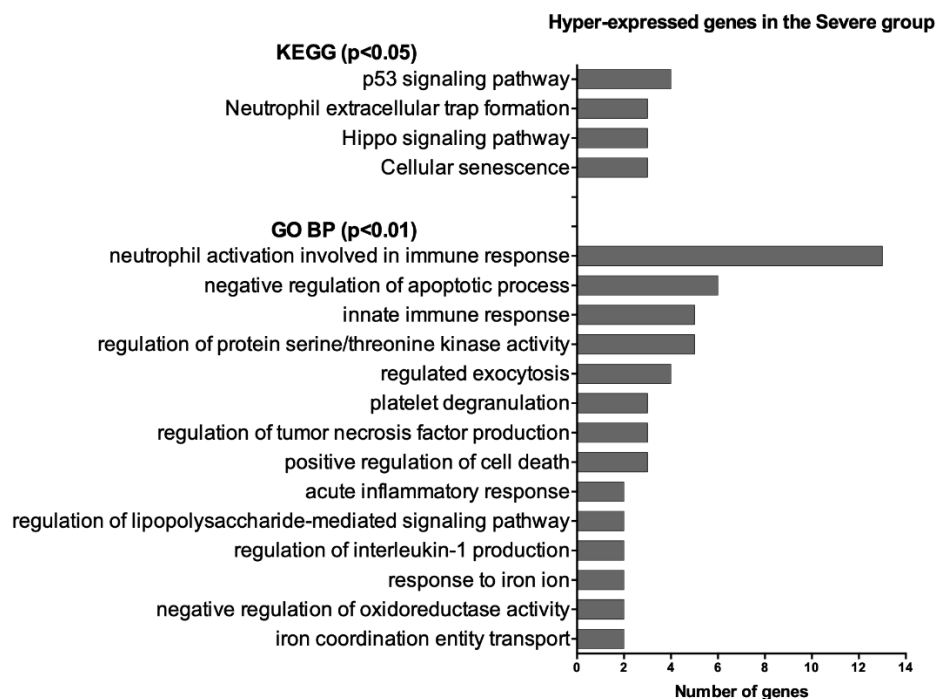
Figure 9. Histogram of enriched GO BP and KEGG pathways terms for the DEGs and hyper-expressed genes in the Severe group. The terms with p < 0.05 were considered significant.

A normalized gene expression analysis (using *GUSB* as an endogenous reference gene) was then performed for the DEGs firstly selected according to KEGG and GO BP enrichment analyses. It was found that 23 genes in the Severe group were significantly (*p* < 0.005) hyper-expressed (**Table 4**). Noteworthy, 17 out of the 23 genes hyper-expressed in the Severe group had been previously reported to be hyper-expressed in the PBMC from COVID-19 patients according to the COVID-19 Related Gene Sets, a database in the Enrichr webtool library [19,77,78] (**Table 4**). Among the 17 genes reported in the COVID-19 Related Gene Sets, ten are related with neutrophil activation in immune response (three are also related with positive regulation of cell death and two with negative regulation of apoptosis), four genes are related with p53 signaling pathway (of which three are also involved in cellular senescence), two genes are related with positive regulation of cell death, and one is related with the Hippo signaling pathway (**Table 4**). Among the six DEGs in the Severe group that were not found as hyper-expressed genes in the COVID-19 Related Gene Sets, two genes are related with neutrophil activation and platelet degranulation, one with neutrophil activation and negative regulation of apoptosis, one with platelet degranulation, and two with the Hippo signaling pathway (**Table 4**). Therefore, 13 out of the 23 genes hyper-expressed in the Severe group are related with neutrophil activation.

Table 4. DEGs selected as potential biomarkers for the Severe group and for the subgroup C. Genes in bold are hyper-expressed in the PBMC from COVID-19 patients (COVID-19 Related Gene Sets/Enrichr database).

| Comparison | DEG | Gene expression | | Database for enrichment analysis |
		Fold-Change	Relative (*p*-value)*	GO BP or KEGG (*in italic*)
Severe x Mild	*LTF*	8.53	0.0001	neutrophil activation involved in immune response; negative regulation of apoptotic process
	HP	6.95	0.0002	neutrophil activation involved in immune response; positive regulation of cell death
	CEACAM8	6.16	0.0009	neutrophil activation involved in immune response
	HPR	5.64	0.0003	acute inflammatory response; positive regulation of cell death
	LCN2	5.02	0.0013	neutrophil activation involved in immune response
	ARG1	4.98	0.0009	neutrophil activation involved in immune response
	GYG1	4.06	0.0002	neutrophil activation involved in immune response
	MPO	4.03	0.0011	neutrophil activation involved in immune response; negative regulation of apoptotic process
	ORM1	3.98	0.0008	neutrophil activation involved in immune response; platelet degranulation
	TXNDC5	3.66	0.0020	neutrophil activation involved in immune response; negative regulation of apoptotic process
	ORM2	3.56	0.0006	neutrophil activation involved in immune response; platelet degranulation
	CAMP	3.27	0.0006	neutrophil activation involved in immune response
	RRM2	2.95	0.0002	p53 signaling pathway
	GGH	2.86	0.0004	neutrophil activation involved in immune response
	SELP	2.71	< 0.0001	platelet degranulation
	CCNB1	2.57	0.0004	**p53 signaling pathway; cellular senescence**
	BMP6	2.43	0.0001	**Hippo signaling pathway**
	BIRC5	2.37	< 0.0001	**Hippo signaling pathway;** negative regulation of apoptotic process
	SNCA	2.33	0.0004	positive regulation of cell death; negative regulation of oxidoreductase activity
	YWHAH	2.25	0.0005	**Hippo signaling pathway**
	CCNB2	2.23	< 0.0001	**p53 signaling pathway; cellular senescence**
	STOM	2.22	0.0004	neutrophil activation involved in immune response
	CDK1	2.14	< 0.0001	**p53 signaling pathway; cellular senescence;** negative regulation of apoptotic process

*t test for relative expression of the DEGs normalized with endogenous reference gene GUSB.

3.3.1. DEGs in the Severe group

The significant fold-change values and the biological functions of all DEGs found for the Severe group (**Figs. 10** and **11** and **Table 4**) clearly show their potentiality as biomarkers associated with COVID-19 severity. Among the seven genes in the GO BP category "neutrophil activation involved in immune response" (**Fig. 10),** three were already

identified as COVID-19 biomarkers: *CEACAM8* (alias CD66B), that codes for a neutrophil cell-adhesion protein and is highly expressed in patients with severe COVID-19 [79]. *ARG1*, coding for arginase 1 and up-regulated in severe cases of COVID-19 [80]; and *LCN2*, which encodes lipocalin 2, a marker of neutrophil activation that was classified by machine learning algorithm as one the most potent discriminators of critical illness in COVID-19 [81]. One DEG in this category, *CAMP*, codify for the antimicrobial molecule cathelicidin (LL37), a modulator of TLR activation and inflammation that has been proposed as a potential candidate for COVID-19 prevention and treatment [82].The remaining three DEGs are related to neutrophil immune functions and metabolism: *STOM*, that codes for stomatin, a membrane protein associated with azurophilic granules [83]; *GGH*, that encodes gamma-glutamyl hydrolase, a lysosomal enzyme involved in the immune response of neutrophils [84]; and *GYGY* that codifies glycogenin, an enzyme involved in the synthesis of glycogen [85].

In the GO BP category "neutrophil activation and positive regulation of cell death" (**Fig.10**) there are two DEGs. One is *HP* that codes for haptoglobin, a hemoglobin-binding plasma protein stored and released by neutrophils in response to activation [86]. Haptoglobin plasmatic levels were shown to correlate with disease severity in COVID-19, being reduced in critical patients [87] and elevated in COVID-19 children [88]. The other DEG, *HPR*, codes for a haptoglobin-related protein that binds hemoglobin was shown to be elevated in the sera of children with bacterial and viral pneumonia [89]. In the GO category "positive regulation of cell death and negative regulation of oxidoreductase activity" there is only one DEG, *SCNA*, which codes for alpha-synuclein, a neuropeptide involved in Parkinson's Disease (PD) that exhibits potent antiviral activity and capacity for signaling the immune system by attracting neutrophils and macrophages and activating dendritic cells [90]. Since oxidative stress, inflammation, and protein aggregation share commonalties between PD and COVID-19 progression, alpha-synuclein is now being investigated at the intersection of PD, SARS-CoV-2 infection, and COVID-19 progression [91].
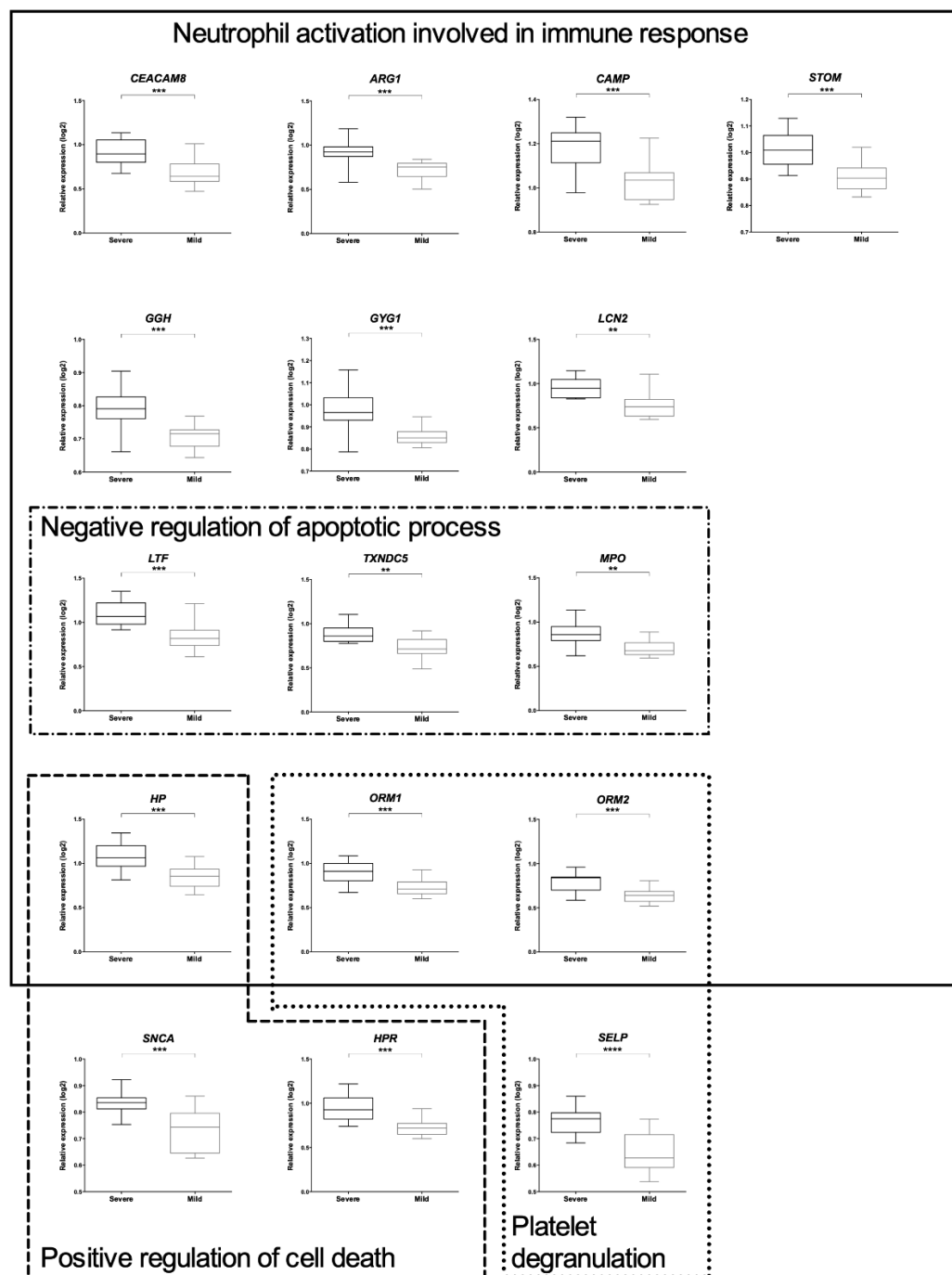
Figure 10. Relative expression of the DEGs related to neutrophil activation, negative regulation of apoptotic process, positive regulation of cell death, and platelet degranulation. The boxplots show the relative expression of genes involved in innate immune response. The relative expression of the differentially expressed genes was normalized with the endogenous reference gene *GUSB* for statistical analysis. Differences were tested using unpaired one-tailed t test (**** *p* < 0.00001; *** *p* < 0.0001; ** *p* < 0.001).
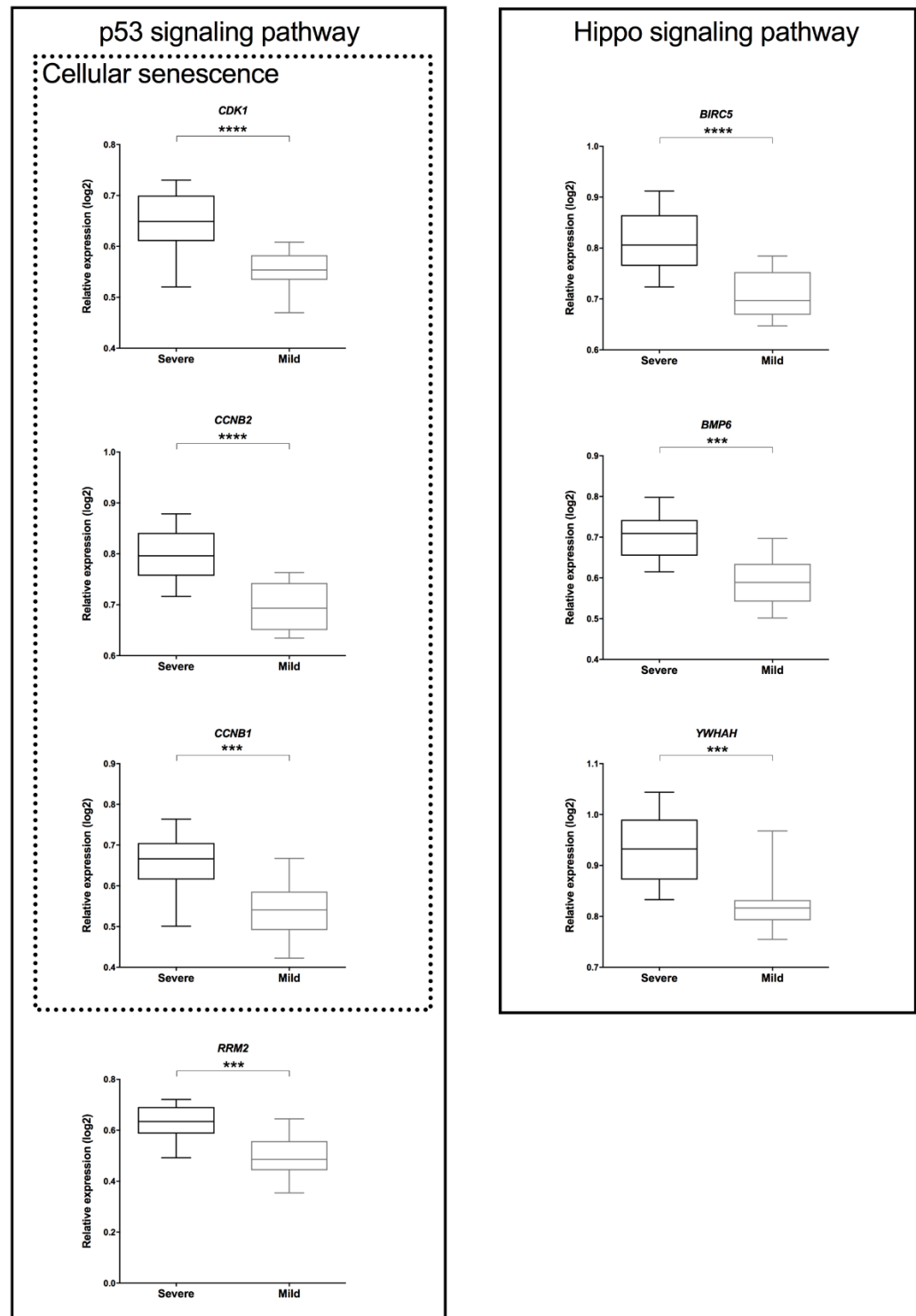
Figure 11. Relative expression of the DEGs related to p53 and Hippo signaling pathways. Boxplots show the relative expression of genes related to cellular senescence or cellular senescence-related signaling pathways. The relative expression of the differentially expressed genes was normalized with the endogenous reference gene *GUSB* for statistical analysis. Differences were tested using unpaired one-tailed t test (**** $p < 0.00001$; *** $p < 0.0001$).

There are three DEGs in the GO BP category "neutrophil activation and negative regulation of apoptosis" (**Fig. 10**). One is *LTF*, which codifies for lactoferrin, a relevant player in innate immunity with antiviral effects against SARS-CoV-2 and a wide range of viral species [92]. Serum levels of lactoferrin were found to be elevated in severe cases of COVID-19 [93]. The other DEG is *MPO*, a gene that codes for myeloperoxidase, a

leukocyte-derived enzyme whose plasmatic levels are elevated in mild to severe cases of COVID-19 and down-regulated in patients with very severe disease [94]. The third gene is *TXND5*, that codes for the thioredoxin domain containing 5 (TXNDC5), an endoplasmic reticulum-resident protein that belongs to the thioredoxin family. The plasmatic levels of this protein are markedly elevated in septic patients, and it has been considered a therapeutic target for attenuating inflammatory responses [95]. Additionally, it was shown that TXND5 is hyper-expressed in B cells after COVID-19 vaccination, being a marker for seroconversion [96]. Therefore, the three genes are potential candidates for monitoring disease severity in COVID-19.

The GO BP category "platelet degranulation and neutrophil activation" has three DEGs (**Fig. 10**). One of these genes is *SELP,* that codes for P-selectin, a platelet cell-adhesion molecule. Increased levels of P-selectin were found in severe cases of COVID-19, what contributes for a prothrombotic state in these patients [97]. The other two genes in this category are *ORM1* and *ORM2*, and both are involved in the encoding of human orosomucoid protein, a major acute-phase plasma protein [98]. Recently, a proteomic analysis of serum from COVID-19 patients showed a significant down-regulation of the ORM1 protein [99].

The KEGG pathway "p53 signaling and cellular senescence" (**Fig. 11**) includes four DEGs. One of these genes is *CDK1* that codes for the cyclin-dependent kinase 1 and is a master regulator of autophagy [100]. *CDK1* was shown to be, through bioinformatics and machine learning approaches, a relevant Hub gene in the WBC transcriptome of COVID-19 patients, with high biomarker and therapeutic target potentials [101]. Other two DEGs in this pathway, *CCNB1* and *CCNB2,* coding respectively for cyclin B1 and cyclin B2, are interactors of *CDK1* and regulate the mammalian cell cycle [102]. The fourth DEG in this pathway, *RRM2*, interacts with *CDK1* and *CNBB1* in the p53 pathway [103] and was recently identified, through bioinformatic analysis, as a key gene in the infection of human intestines by SARS-CoV-2 [104].

Finally, there are three DEGs in the KEGG "Hippo signaling pathway" (**Fig. 11**). One of these genes is *BIRC5* that codes for survivin, an inhibitor of apoptosis protein. Survivin is indispensable for the homeostasis of the immune system, being required for innate and adaptive immune responses, differentiation of CD4+ and CD8+ memory T-cells, and for B cell maturation [105]. The other two DEGs are *BMP6* and *YWHAH*. The former codes for the bone morphogenetic protein 6, a regulator of vascular homeostasis and angiogenesis [106] recently identified as an anti-inflammatory cytokine [107]. The latter codes for the 14-3-3η (eta) protein, a phospho-serine/phospho-threonine binding protein that interacts with a wide range of protein targets and participates in multiple cellular biological functions. The 14-3-3η protein is involved in the modulation of antiviral defenses via the RLR signaling pathway. The interaction between 14-3-3η and the melanoma differentiation-associated gene 5 (*MDA5*) accelerates the activation of the MDA5 signaling, thus helping host cells to mount an effective response against RNA viral infections [108].

3.4. Subnetworks for module genes and DEGs

Subnetworks were constructed for the yellow and magenta modules– both positively correlated with the Severe group - using genes enriched for innate immune response and inflammation processes and pathways. The subnetwork for the black module, positively correlated with subgroup A, was constructed using genes enriched for inflammation, innate immune response, and immune response regulation. All these genes and their respective functions are listed in **Table S9**. The DEGs identified in the Severe *vs.* Mild group comparison were also included in the yellow and magenta subnetworks (**Table S8).** Consequently, these GCNs were constructed with 141 genes for the yellow subnetwork, 45 genes for the magenta subnetwork, and 33 genes for the black subnetwork. For all GCNs a gene-gene link cut-off of r>|0.9| was adopted. The yellow and magenta GCNs (**Figs. 12** and **13**) for the Severe group showed a higher value of connectivity (10.6 for the yellow and 6.5 for the magenta) when compared with the GCNs obtained for the Mild group (3.2 for the yellow and 2.3 for the magenta). The GCNs for the black module (**Fig. 14**) showed

a higher connectivity for subgroup A (11.3) when compared with the subgroup B (6.0). Additionally, more genes are interconnected in the yellow GCN for the Severe group (104 genes and 551 links) than in the network for the Mild group (74 genes and 241 links). It is worth to mention that the yellow GCN for the Severe group encompasses several genes involved in neutrophil activation (**Fig. 12**). Similarly, the black GCN for subgroup A contains many genes involved in the I-kappaB Kinase/NF-kappaB signaling, an important modulator of inflammatory and immune responses (**Fig. 14**).
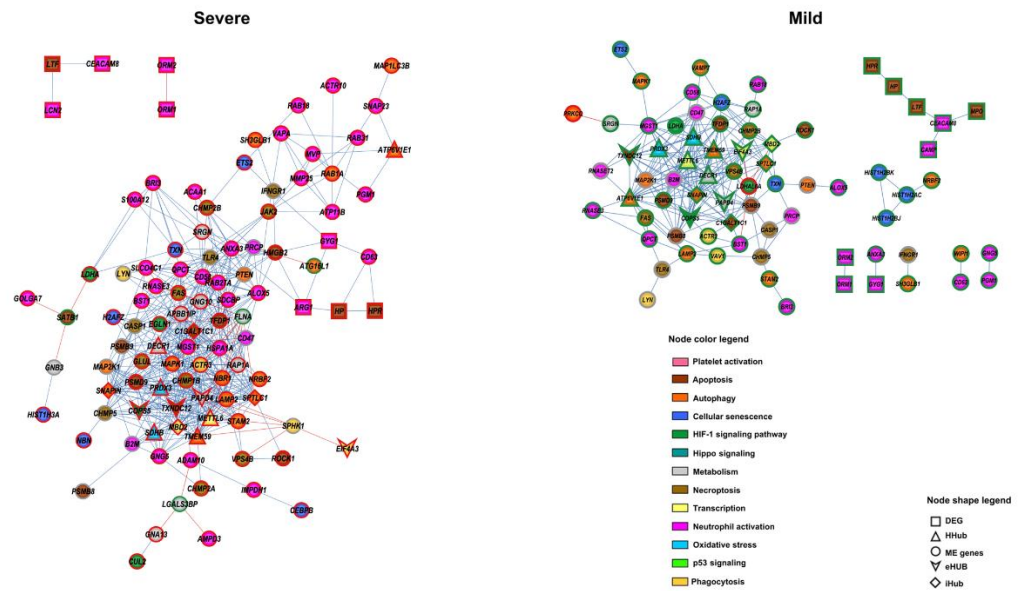
Figure 12. Subnetworks for the yellow module containing ME genes and DEGs for the Severe and Mild groups. Red or blue links indicate positive or negative expression correlation values, respectively. Red or green border colors account for hyperexpressed or hypoexpressed genes, respectively.
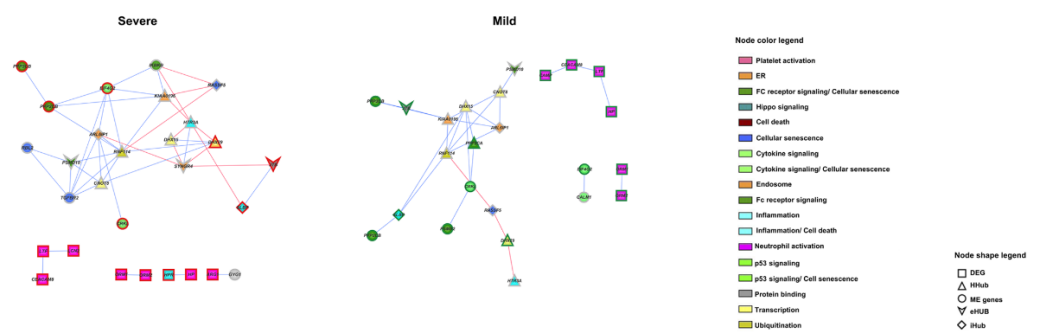

Figure 13. Subnetworks for the magenta module containing ME genes and DEGs for the Severe and Mild groups. Red or blue links indicate positive or negative expression correlation values, respectively. Red or green border colors account for hyperexpressed or hypoexpressed genes, respectively.
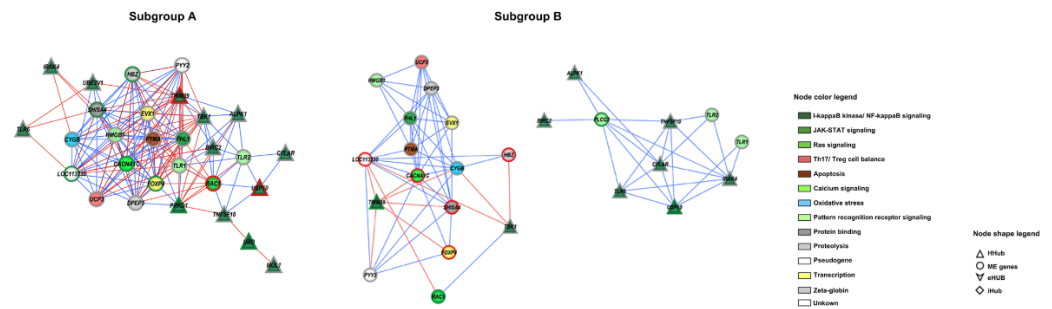
Figure 14. Subnetworks for the black module containing ME genes and DEGs for the subgroups A and B. Red or blue links indicate positive or negative expression correlation values, respectively. Red or green border colors account for hyperexpressed or hypoexpressed genes, respectively.

4. Discussion

In this work, we investigated the transcriptional response of human leukocytes to SARS-CoV-2 infection focusing on the differences between mild and severe cases and between age subgroups (younger and older adults) through the functional analysis of transcriptional modules (WGCNA) and the identification of differentially expressed genes.

The Severe and Mild groups presented distinct transcriptional profiles. The functional characterization of the transcriptional modules, accomplished through gene enrichment analysis, showed that two of these modules, yellow and magenta, both positively associated with the Severe group, are involved in inflammation and immune response processes, such as neutrophil activation, necroptosis, autophagy, phagocytosis, and cellular senescence. Expectedly, these two modules contain many hub genes – which are important for maintaining the robustness of the transcriptional modules and of the gene co-expression network [16-18] - related to those processes (**Table 3**). The black module, positively associated with the subgroup A, which encompass the severe young patients, contains many hubs related to the recognition and response to viral infections, as well as hubs related to modulatory mechanisms acting on inflammatory and immune responses (**Table 3** and **Fig. 8**).

The construction of subnetworks for the yellow, magenta, and black modules, using genes enriched for innate immune response, inflammation, immunoregulation and DEGs (Severe vs. Mild comparison), helped to further characterize the genomic mechanisms related to disease severity and age in our patients. The analysis of the yellow subnetwork showed that most of the highly interconnected genes in the Severe group are hyper-expressed and that many of these genes are involved in neutrophil activation, with other genes involved in necroptosis, apoptosis, and autophagy (**Fig. 12**). This high network connectivity indicates that in the Severe group the biological functions and/or cellular processes related to innate immune response and inflammation are more activated than in the Mild group, shedding some light on the underlying genomic mechanism, since the immune response to SARS-CoV-2 is characterized by neutrophil hyperactivation and high neutrophil counts [109].

Most of the patients in the Severe group presented fever, dyspnea, wheezing in the chest, chills, and vomiting, while in the Mild group a sizable number of patients solely presented mild symptoms, such as coryza and headache (**Table 1**). It is well known that if the response to respiratory viruses is inadequate the infection spreads to lower respiratory tract (LRT) [110]. An early and effective immune response in patients infected with SARS-CoV-2 can limit and eliminate the infection yet in the upper respiratory tract (URT) [111]. Moreover, genomic analyses shown that there is no tissue specific genetic adaptation of SARS-CoV-2 to patients' URT or LRT [112]. Therefore, the transcriptional differences between the Severe and Mild groups reflect and are coherent with the different presentation of symptoms and with the LRT infection and severe COVID-19.

In the Severe group we found genomic differences between the subgroup A, constituted by adolescents and young adults, and the subgroup B, the older adults. The magenta and black transcriptional modules, both positively associated with the subgroup A,

contain many HH genes related to the modulation of inflammatory and immune responses, as described in the Results section. Moreover, in the black subnetworks the highest gene interconnectivity was found for subgroup A (**Fig. 14**), thus indicating that immune modulatory functions are more activated in this subgroup when compared to subgroup B. These findings may help to explain the better disease course and faster recovery observed in younger COVID-19 patients, while in the elderly patients a less effective immune modulation of COVID-19, allied to immune senescence and, eventually, to comorbidities, would lead to a worse outcome [113-115].

A comparative gene expression analysis between the Severe and Mild groups, followed by subsequent gene enrichment and normalized gene expression analyses, identified 23 genes significantly hyper-expressed in the Severe group, of which 17 were previously reported as hyper-expressed in the PBMC of COVID-19 patients. The functional characterization by GO BP and KEGG enrichment analyses of these differentially expressed genes (DEGs) is presented in **Table 4** and **Figs. 10** and **11**. Most of them - 13 out of 23 - are related to neutrophil activation (three are also related with positive regulation of cell death, two with negative regulation of apoptosis, and two with platelet degranulation), four genes are related to p53 signaling pathway (three are also related to cellular senescence), three to Hippo signaling, two are related to the positive regulation of cell death and one solely to platelet degranulation. This functional profile is rather expectable considering the hemogram-derived ratios between the Severe and Mild groups (**Table 2**).

Among the 23 DEGs significantly hyper-expressed in the Severe group, ten had been previously proposed as potential COVID-19 biomarkers and/or therapeutic targets, as described in the Results section. Eight of them are related to neutrophil activation (*LTF*, *ARG1*, *CEACAM8*, *LCN2*, *MPO*, *CAMP*, *ORM1*, *TXND5*), one to platelet degranulation (SELP), and one to p53 signaling pathway and cellular senescence (*CDK1*). As shown in **Table 4**, seven of these genes already figured as hyper-expressed in the PBMC from COVID-19 patients in the COVID-19 Related Gene Set/Enrichr database.

Here we reported 13 new potential transcriptional biomarkers (see Results for further details and references), all hyper-expressed in the peripheral blood leukocytes of severe adult COVID-19 patients (**Figs. 10** and **11**). Two of these genes are *HP* (haptoglobin) and *HPR* (haptoglobin-related protein), both involved in the positive regulation of cell death, and formerly associated, respectively, with COVID-19 in children, and with bacterial and viral pneumonia in children. Four genes are involved in neutrophil activation, namely *GGH*, *GYG1*, *ORM2* and *STOM*, and were not yet described as potential COVID-19 markers. Three other potential transcriptional markers belong to the Hippo signaling pathway: *BIRC5*, which codes for the anti-apoptotic protein Survivin, *BMP6*, that codes for the bone morphogenetic protein 6, an anti-inflammatory cytokine, and *YWHAH*, coding for a chaperone involved in the modulation of antiviral responses. In the p53 signaling and cellular senescence pathway there are three new potential biomarkers: *CCNB1* and *CCNB2*, coding for cyclin B1 and B2 respectively, and *RRM2*, that interacts with *CCNB1* and *CDK1* in the p53 pathway. Lastly, there is *SNCA*, a gene that codes for alpha-synuclein, a neuropeptide involved in Parkinson's Disease (PD) with antiviral activity. As we mentioned before, alpha-synuclein is being investigated at the intersection of PD, SARS-CoV-2, and COVID-19 [91].

5. Conclusions

The investigation of blood leukocyte transcriptional response to SARS-CoV-2 infection - focused on the differences between mild and severe cases, and between age subgroups (adolescents/younger and older adults) - led to the characterization of transcriptional modules associated to age and severity traits, and to the identification of differentially expressed genes that are new potential biomarkers and/or therapeutic targets for COVID-19.

Supplementary Materials: The following supporting information can be downloaded at: www.mdpi.com/xxx/s1, Supplementary Methods: Relative gene expression analysis; Figure S1:

Factor Analysis of Mixed Data; Figure S2: Selection of the soft-thresholding power (β); Figure S3: Module-trait relationships (complete report); Figure S4: Intramodular node categorization; Table S1: Clinical and demographic data of the 121 patients; Table S2: Clinical and demographic data of the patients included in the transcriptomic analyses; Table S3: Selection of the endogenous reference gene most appropriate to our study; Table S4: Reference values and range of the hemogram parameters used in this study; Table S5: Enrichment analyses for the yellow module; Table S6: Enrichment analyses for the magenta module; Table S7: Enrichment analyses for the black module; Table S8: Enrichment analyses for DEGs obtained from the Severe *vs* Mild group comparison; Table S9: List of the genes used for the construction of the modules' subnetworks.

References

1. Vieira, S.E.; Bando, S.Y.; Lauterbach, G.D.P.; Moreira-Filho, C.A. Human Leukocyte Transcriptional Response to SARS-CoV-2 Infection. *Clinics (Sao Paulo)* **2020**, *75*, e2078, doi:10.6061/clinics/2020/e2078.

2. Yang, X.; Rutkovsky, A.C.; Zhou, J.; Zhong, Y.; Reese, J.; Schnell, T.; Albrecht, H.; Owens, W.B.; Nagarkatti, P.S.; Nagarkatti, M. Characterization of Altered Gene Expression and Histone Methylation in Peripheral Blood Mononuclear Cells Regulating Inflammation in COVID-19 Patients. *J Immunol* **2022**, *208*, 1968-1977, doi:10.4049/jimmunol.2101099.

3. Kissler, S.M.; Tedijanto, C.; Goldstein, E.; Grad, Y.H.; Lipsitch, M. Projecting the transmission dynamics of SARS-CoV-2 through the postpandemic period. *Science* **2020**, *368*, 860-868, doi:10.1126/science.abb5793.

4. Langfelder, P.; Zhang, B.; Horvath, S. Dynamic Tree Cut: in-depth description, tests and applications. Available online: http://www.genetics.ucla.edu/labs/horvath/CoexpressionNetwork/BranchCutting (accessed on October, 21).

5. Naveca, F.G.; Nascimento, V.; de Souza, V.C.; Corado, A.L.; Nascimento, F.; Silva, G.; Costa, Á.; Duarte, D.; Pessoa, K.; Mejía, M.; et al. COVID-19 in Amazonas, Brazil, was driven by the persistence of endemic lineages and P.1 emergence. *Nat Med* **2021**, *27*, 1230-1238, doi:10.1038/s41591-021-01378-7.

6. Faria, N.R.; Mellan, T.A.; Whittaker, C.; Claro, I.M.; Candido, D.D.S.; Mishra, S.; Crispim, M.A.E.; Sales, F.C.S.; Hawryluk, I.; McCrone, J.T.; et al. Genomics and epidemiology of the P.1 SARS-CoV-2 lineage in Manaus, Brazil. *Science* **2021**, *372*, 815-821, doi:10.1126/science.abh2644.

7. Pagès, J. Analyse factorielle de données mixtes. *Revue de Statistique Appliquée* **2004**, *52*, 19.

8.   Lê, S.; Josse, J.; Husson, F. FactoMineR: An R Package for Multivariate Analysis. *2008 %9 %! FactoMineR: An R Package for Multivariate Analysis* **2008**, *25*, 18, doi:10.18637/jss.v025.i01 %& 1.

9.   Team, R.C. R: A language and environment for statistical computing. Available online: http://www.R-project.org/. (accessed on

10.   Velazquez, S.; Madurga, R.; Castellano, J.M.; Rodriguez-Pascual, J.; de Aguiar Diaz Obregon, S.R.; Jimeno, S.; Montero, J.I.; Wichner, P.S.V.; López-Escobar, A. Hemogram-derived ratios as prognostic markers of ICU admission in COVID-19. *BMC Emerg Med* **2021**, *21*, 89, doi:10.1186/s12873-021-00480-w.

11.   Corman, V.M.; Landt, O.; Kaiser, M.; Molenkamp, R.; Meijer, A.; Chu, D.K.; Bleicker, T.; Brünink, S.; Schneider, J.; Schmidt, M.L.; et al. Detection of 2019 novel coronavirus (2019-nCoV) by real-time RT-PCR. *Euro Surveill* **2020**, *25*, doi:10.2807/1560-7917.ES.2020.25.3.2000045.

12.   Sakthivel, S.K.; Whitaker, B.; Lu, X.; Oliveira, D.B.; Stockman, L.J.; Kamili, S.; Oberste, M.S.; Erdman, D.D. Comparison of fast-track diagnostics respiratory pathogens multiplex real-time RT-PCR assay with in-house singleplex assays for comprehensive detection of human respiratory viruses. *J Virol Methods* **2012**, *185*, 259-266, doi:10.1016/j.jviromet.2012.07.010.

13.   Smyth, G.K. Limma: linear models for microarray data. In *Bioinformatics and Computational Biology Solutions Using R and Bioconductor.*, Gentleman, V., Carey, S., Dudoit, R. & Irizarry, W.H., Ed.; Springer: NewYork, 2005; pp. 397-420.

14.   Ritchie, M.E.; Phipson, B.; Wu, D.; Hu, Y.; Law, C.W.; Shi, W.; Smyth, G.K. limma powers differential expression analyses for RNA-sequencing and microarray studies. *Nucleic Acids Res* **2015**, *43*, e47, doi:10.1093/nar/gkv007.

15.   Langfelder, P.; Horvath, S. WGCNA: an R package for weighted correlation network analysis. *BMC Bioinformatics* **2008**, *9*, 559, doi:10.1186/1471-2105-9-559.

16.   Barabási, A.L.; Gulbahce, N.; Loscalzo, J. Network medicine: a network-based approach to human disease. *Nat Rev Genet* **2011**, *12*, 56-68, doi:10.1038/nrg2918.

17.   Bando, S.Y.; Bertonha, F.B.; Pimentel-Silva, L.R.; de Oliveira, J.G.M.; Carneiro, M.A.D.; Oku, M.H.M.; Wen, H.T.; Castro, L.H.M.; Moreira-Filho, C.A. Hippocampal CA3 transcriptional modules associated with granule cell alterations and cognitive impairment in refractory mesial temporal lobe epilepsy patients. *Sci Rep* **2021**, *11*, 10257, doi:10.1038/s41598-021-89802-3.

18.   van Dam, S.; Võsa, U.; van der Graaf, A.; Franke, L.; de Magalhães, J.P. Gene co-expression analysis for functional classification and gene-disease predictions. *Brief Bioinform* **2018**, *19*, 575-592, doi:10.1093/bib/bbw139.

19.   Kuleshov, M.V.; Jones, M.R.; Rouillard, A.D.; Fernandez, N.F.; Duan, Q.; Wang, Z.; Koplev, S.; Jenkins, S.L.; Jagodnik, K.M.; Lachmann, A.; et al. Enrichr: a comprehensive gene set enrichment analysis web server 2016 update. *Nucleic Acids Res* **2016**, *44*, W90-97, doi:10.1093/nar/gkw377.

20.   Shannon, P.; Markiel, A.; Ozier, O.; Baliga, N.S.; Wang, J.T.; Ramage, D.; Amin, N.; Schwikowski, B.; Ideker, T. Cytoscape: a software environment for integrated models of biomolecular interaction networks. *Genome Res* **2003**, *13*, 2498-2504, doi:10.1101/gr.1239303.

21.   Zhang, Y.; Wang, S.; Xia, H.; Guo, J.; He, K.; Huang, C.; Luo, R.; Chen, Y.; Xu, K.; Gao, H.; et al. Identification of Monocytes Associated with Severe COVID-19 in the PBMCs of Severely Infected patients Through Single-Cell Transcriptome Sequencing. *Engineering (Beijing)* **2021**, doi:10.1016/j.eng.2021.05.009.

22.   Tian, M.; Liu, W.; Li, X.; Zhao, P.; Shereen, M.A.; Zhu, C.; Huang, S.; Liu, S.; Yu, X.; Yue, M.; et al. HIF-1α promotes SARS-CoV-2 infection and aggravates inflammatory responses to COVID-19. *Signal Transduct Target Ther* **2021**, *6*, 308, doi:10.1038/s41392-021-00726-w.

23.   Ma, Y.; Zhang, Y.; Zhu, L. Role of neutrophils in acute viral infection. *Immun Inflamm Dis* **2021**, doi:10.1002/iid3.500.

24.   Lotfi, R.; Kalmarzi, R.N.; Roghani, S.A. A review on the immune responses against novel emerging coronavirus (SARS-CoV-2). *Immunol Res* **2021**, *69*, 213-224, doi:10.1007/s12026-021-09198-0.

25.   Liu, Z.; Ning, J.; Zheng, X.; Meng, J.; Han, L.; Zheng, H.; Zhong, L.; Chen, X.F.; Zhang, X.; Luo, H.; et al. TMEM59 interacts with TREM2 and modulates TREM2-dependent microglial activities. *Cell Death Dis* **2020**, *11*, 678, doi:10.1038/s41419-020-02874-3.

26.   Guo, H.; Chitiprolu, M.; Roncevic, L.; Javalet, C.; Hemming, F.J.; Trung, M.T.; Meng, L.; Latreille, E.; Tanese de Souza, C.; McCulloch, D.; et al. Atg5 Disassociates the V 1 V 0 -ATPase to Promote Exosome Production and Tumor Metastasis Independent of Canonical Macroautophagy. *Dev Cell* **2017**, *43*, 716-730.e717, doi:10.1016/j.devcel.2017.11.018.

27.   Lauterbach, M.A.; Saavedra, V.; Mangan, M.S.J.; Penno, A.; Thiele, C.; Latz, E.; Kuerschner, L. 1-Deoxysphingolipids cause autophagosome and lysosome accumulation and trigger NLRP3 inflammasome activation. *Autophagy* **2021**, *17*, 1947-1961, doi:10.1080/15548627.2020.1804677.

28.   Shi, B.; Huang, Q.Q.; Birkett, R.; Doyle, R.; Dorfleutner, A.; Stehlik, C.; He, C.; Pope, R.M. SNAPIN is critical for lysosomal acidification and autophagosome maturation in macrophages. *Autophagy* **2017**, *13*, 285-301, doi:10.1080/15548627.2016.1261238.

29.   Lee, Y.J. Knockout Mouse Models for Peroxiredoxins. *Antioxidants (Basel)* **2020**, *9*, doi:10.3390/antiox9020182.

30.   Lemarie, A.; Huc, L.; Pazarentzos, E.; Mahul-Mellier, A.L.; Grimm, S. Specific disintegration of complex II succinate:ubiquinone oxidoreductase links pH changes to oxidative stress for apoptosis induction. *Cell Death Differ* **2011**, *18*, 338-349, doi:10.1038/cdd.2010.93.

31.   Jeong, W.; Lee, D.Y.; Park, S.; Rhee, S.G. ERp16, an endoplasmic reticulum-resident thiol-disulfide oxidoreductase: biochemical properties and role in apoptosis induced by endoplasmic reticulum stress. *J Biol Chem* **2008**, *283*, 25557-25566, doi:10.1074/jbc.M803804200.

32.   Tanimura, A.; Miyoshi, K.; Horiguchi, T.; Hagita, H.; Fujisawa, K.; Noma, T. Mitochondrial Activity and Unfolded Protein Response are Required for Neutrophil Differentiation. *Cell Physiol Biochem* **2018**, *47*, 1936-1950, doi:10.1159/000491464.

33.   Jiang, Y.; Wen, T.; Yan, R.; Kim, S.R.; Stowell, S.R.; Wang, W.; Wang, Y.; An, G.; Cummings, R.D.; Ju, T. O-glycans on death receptors in cells modulate their sensitivity to TRAIL-induced apoptosis through affecting on their stability and oligomerization. *FASEB J* **2020**, *34*, 11786-11801, doi:10.1096/fj.201900053RR.

34.   Peteranderl, C.; Herold, S. The Impact of the Interferon/TNF-Related Apoptosis-Inducing Ligand Signaling Axis on Disease Progression in Respiratory Viral Infection and Beyond. *Front Immunol* **2017**, *8*, 313, doi:10.3389/fimmu.2017.00313.

35.   Chen, T.C.; Tallo-Parra, M.; Cao, Q.M.; Kadener, S.; Böttcher, R.; Pérez-Vilaró, G.; Boonchuen, P.; Somboonwiwat, K.; Díez, J.; Sarnow, P. Host-derived circular RNAs display proviral activities in Hepatitis C virus-infected cells. *PLoS Pathog* **2020**, *16*, e1008346, doi:10.1371/journal.ppat.1008346.

36.   Snoek, B.C.; Babion, I.; Koppers-Lalic, D.; Pegtel, D.M.; Steenbergen, R.D. Altered microRNA processing proteins in HPV-induced cancers. *Curr Opin Virol* **2019**, *39*, 23-32, doi:10.1016/j.coviro.2019.07.002.

37.   Reusch, N.; De Domenico, E.; Bonaguro, L.; Schulte-Schrepping, J.; Baßler, K.; Schultze, J.L.; Aschenbrenner, A.C. Neutrophils in COVID-19. *Front Immunol* **2021**, *12*, 652470, doi:10.3389/fimmu.2021.652470.

38.   Murdaca, G.; Di Gioacchino, M.; Greco, M.; Borro, M.; Paladin, F.; Petrarca, C.; Gangemi, S. Basophils and Mast Cells in COVID-19 Pathogenesis. *Cells* **2021**, *10*, doi:10.3390/cells10102754.

39.   Clark, A.R.; Ohlmeyer, M. Protein phosphatase 2A as a therapeutic target in inflammation and neurodegeneration. *Pharmacol Ther* **2019**, *201*, 181-201, doi:10.1016/j.pharmthera.2019.05.016.

40.   Rodriguez, M.S.; Egaña, I.; Lopitz-Otsoa, F.; Aillet, F.; Lopez-Mato, M.P.; Dorronsoro, A.; Dorronroso, A.; Lobato-Gil, S.; Sutherland, J.D.; Barrio, R.; et al. The RING ubiquitin E3 RNF114 interacts with A20 and modulates NF-κB activity and T-cell activation. *Cell Death Dis* **2014**, *5*, e1399, doi:10.1038/cddis.2014.366.

41.   Herr, N.; Bode, C.; Duerschmied, D. The Effects of Serotonin in Immune Cells. *Front Cardiovasc Med* **2017**, *4*, 48, doi:10.3389/fcvm.2017.00048.

42.   Schoenichen, C.; Bode, C.; Duerschmied, D. Role of platelet serotonin in innate immune cell recruitment. *Front Biosci (Landmark Ed)* **2019**, *24*, 514-526, doi:10.2741/4732.

43.   Soria-Castro, R.; Meneses-Preza, Y.G.; Rodríguez-López, G.M.; Romero-Ramírez, S.; Sosa-Hernández, V.A.; Cervantes-Díaz, R.; Pérez-Fragoso, A.; Torres-Ruíz, J.J.; Gómez-Martín, D.; Campillo-Navarro, M.; et al. Severe COVID-19 is marked by

dysregulated serum levels of carboxypeptidase A3 and serotonin. *J Leukoc Biol* **2021**, *110*, 425-431, doi:10.1002/JLB.4HI0221-087R.

44.   Pattabhi, S.; Knoll, M.L.; Gale, M.; Loo, Y.M. DHX15 Is a Coreceptor for RLR Signaling That Promotes Antiviral Defense Against RNA Virus Infection. *J Interferon Cytokine Res* **2019**, *39*, 331-346, doi:10.1089/jir.2018.0163.

45.   Zhu, Q.; Tan, P.; Li, Y.; Lin, M.; Li, C.; Mao, J.; Cui, J.; Zhao, W.; Wang, H.Y.; Wang, R.F. DHX29 functions as an RNA co-sensor for MDA5-mediated EMCV-specific antiviral immunity. *PLoS Pathog* **2018**, *14*, e1006886, doi:10.1371/journal.ppat.1006886.

46.   Derivery, E.; Gautreau, A. Evolutionary conservation of the WASH complex, an actin polymerization machine involved in endosomal fission. *Commun Integr Biol* **2010**, *3*, 227-230, doi:10.4161/cib.3.3.11185.

47.   Bouhaddou, M.; Memon, D.; Meyer, B.; White, K.M.; Rezelj, V.V.; Correa Marrero, M.; Polacco, B.J.; Melnyk, J.E.; Ulferts, S.; Kaake, R.M.; et al. The Global Phosphorylation Landscape of SARS-CoV-2 Infection. *Cell* **2020**, *182*, 685-712.e619, doi:10.1016/j.cell.2020.06.034.

48.   Akiyama, T.; Suzuki, T.; Yamamoto, T. RNA decay machinery safeguards immune cell development and immunological responses. *Trends Immunol* **2021**, *42*, 447-460, doi:10.1016/j.it.2021.03.008.

49.   Li, J.; Guo, S.; Chai, F.; Sun, Q.; Li, P.; Gao, L.; Dai, L.; Ouyang, X.; Zhou, Z.; Zhou, L.; et al. Genetically incorporated crosslinkers reveal NleE attenuates host autophagy dependent on PSMD10. *Elife* **2021**, *10*, doi:10.7554/eLife.69047.

50.   Marques, R.F.; Duncan, K.E. SYNGR4 and PLEKHB1 deregulation in motor neurons of amyotrophic lateral sclerosis models: potential contributions to pathobiology. *Neural Regen Res* **2022**, *17*, 266-270, doi:10.4103/1673-5374.317960.

51.   Srivastava, N.; Lacy, P. Trafficking of TNF via recycling endosomes in neutrophils. *ll Asth Clin Immun* **2014**, *10*, A*47*, doi:10.1186/1710-1492-10-S2-A47.

52.   Kanome, T.; Itoh, N.; Ishikawa, F.; Mori, K.; Kim-Kaneyama, J.R.; Nose, K.; Shibanuma, M. Characterization of Jumping translocation breakpoint (JTB) gene product isolated as a TGF-beta1-inducible clone involved in regulation of mitochondrial function, cell growth and cell death. *Oncogene* **2007**, *26*, 5991-6001, doi:10.1038/sj.onc.1210423.

53.   Medini, H.; Zirman, A.; Mishmar, D. Immune system cells from COVID-19 patients display compromised mitochondrial-nuclear expression co-regulation and rewiring toward glycolysis. *iScience* **2021**, *24*, 103471, doi:10.1016/j.isci.2021.103471.

54.   Li, M.; Tucker, L.D.; Asara, J.M.; Cheruiyot, C.K.; Lu, H.; Wu, Z.J.; Newstein, M.C.; Dooner, M.S.; Friedman, J.; Lally, M.A.; et al. Stem-loop binding protein is a multifaceted cellular regulator of HIV-1 replication. *J Clin Invest* **2016**, *126*, 3117-3129, doi:10.1172/JCI82360.

55.   Donninger, H.; Schmidt, M.L.; Mezzanotte, J.; Barnoud, T.; Clark, G.J. Ras signaling through RASSF proteins. *Semin Cell Dev Biol* **2016**, *58*, 86-95, doi:10.1016/j.semcdb.2016.06.007.

56.   Dong, R.; Zhu, T.; Benedetti, L.; Gowrishankar, S.; Deng, H.; Cai, Y.; Wang, X.; Shen, K.; De Camilli, P. The inositol 5-phosphatase INPP5K participates in the fine control of ER organization. *J Cell Biol* **2018**, *217*, 3577-3592, doi:10.1083/jcb.201802125.

57.   Zhang, Y.; Chen, S.; Jin, Y.; Ji, W.; Zhang, W.; Duan, G. An Update on Innate Immune Responses during SARS-CoV-2 Infection. *Viruses* **2021**, *13*, doi:10.3390/v13102060.

58.   Zheng, M.; Karki, R.; Williams, E.P.; Yang, D.; Fitzpatrick, E.; Vogel, P.; Jonsson, C.B.; Kanneganti, T.D. TLR2 senses the SARS-CoV-2 envelope protein to produce inflammatory cytokines. *Nat Immunol* **2021**, *22*, 829-838, doi:10.1038/s41590-021-00937-x.

59.   Solt, L.A.; May, M.J. The IkappaB kinase complex: master regulator of NF-kappaB signaling. *Immunol Res* **2008**, *42*, 3-18, doi:10.1007/s12026-008-8025-1.

60.   Liu, T.; Zhang, L.; Joo, D.; Sun, S.C. NF-κB signaling in inflammation. *Signal Transduct Target Ther* **2017**, *2*, doi:10.1038/sigtrans.2017.23.

61.   Robert, V.; Triffaux, E.; Paulet, P.E.; Guéry, J.C.; Pelletier, L.; Savignac, M. Protein kinase C-dependent activation of CaV1.2 channels selectively controls human TH2-lymphocyte functions. *J Allergy Clin Immunol* **2014**, *133*, 1175-1183, doi:10.1016/j.jaci.2013.10.038.

62.   Tong, L.; Tergaonkar, V. Rho protein GTPases and their interactions with NFκB: crossroads of inflammation and matrix biology. *Biosci Rep* **2014**, *34*, doi:10.1042/BSR20140021.

63.   Yu, K.; He, J.; Wu, Y.; Xie, B.; Liu, X.; Wei, B.; Zhou, H.; Lin, B.; Zuo, Z.; Wen, W.; et al. Dysregulated adaptive immune response contributes to severe COVID-19. *Cell Res* **2020**, *30*, 814-816, doi:10.1038/s41422-020-0391-9.

64.   Wiehagen, K.R.; Corbo-Rodgers, E.; Li, S.; Staub, E.S.; Hunter, C.A.; Morrisey, E.E.; Maltzman, J.S. Foxp4 is dispensable for T cell development, but required for robust recall responses. *PLoS One* **2012**, *7*, e42273, doi:10.1371/journal.pone.0042273.

65.   O'Connor, E.B.; Muñoz-Wolf, N.; Leon, G.; Lavelle, E.C.; Mills, K.H.G.; Walsh, P.T.; Porter, R.K. UCP3 reciprocally controls CD4+ Th17 and Treg cell differentiation. *PLoS One* **2020**, *15*, e0239713, doi:10.1371/journal.pone.0239713.

66.   De Biasi, S.; Meschiari, M.; Gibellini, L.; Bellinazzi, C.; Borella, R.; Fidanza, L.; Gozzi, L.; Iannone, A.; Lo Tartaro, D.; Mattioli, M.; et al. Marked T cell activation, senescence, exhaustion and skewing towards TH17 in patients with COVID-19 pneumonia. *Nat Commun* **2020**, *11*, 3434, doi:10.1038/s41467-020-17292-4.

67.   Ou, L.; Li, X.; Chen, B.; Ge, Z.; Zhang, J.; Zhang, Y.; Cai, G.; Li, Z.; Wang, P.; Dong, W. Recombinant Human Cytoglobin Prevents Atherosclerosis by Regulating Lipid Metabolism and Oxidative Stress. *J Cardiovasc Pharmacol Ther* **2018**, *23*, 162-173, doi:10.1177/1074248417724870.

68.   Wei, X.; Zhang, H. Four and a half LIM domains protein 1 can be as a double-edged sword in cancer progression. *Cancer Biol Med* **2020**, *17*, 270-281, doi:10.20892/j.issn.2095-3941.2019.0420.

69.   Zhou, Z.; Lu, J.; Dou, J.; Lv, Z.; Qin, X.; Lin, J. FHL1 and Smad4 synergistically inhibit vascular endothelial growth factor expression. *Mol Med Rep* **2013**, *7*, 649-653, doi:10.3892/mmr.2012.1202.

70.   Kong, Y.; Han, J.; Wu, X.; Zeng, H.; Liu, J.; Zhang, H. VEGF-D: a novel biomarker for detection of COVID-19 progression. *Crit Care* **2020**, *24*, 373, doi:10.1186/s13054-020-03079-y.

71.   Zhu, M.; Settele, F.; Kotak, S.; Sanchez-Pulido, L.; Ehret, L.; Ponting, C.P.; Gönczy, P.; Hoffmann, I. MISP is a novel Plk1 substrate required for proper spindle orientation and mitotic progression. *J Cell Biol* **2013**, *200*, 773-787, doi:10.1083/jcb.201207050.

72.   Briata, P.; Van De Werken, R.; Airoldi, I.; Ilengo, C.; Di Blas, E.; Boncinelli, E.; Corte, G. Transcriptional repression by the human homeobox protein EVX1 in transfected mammalian cells. *J Biol Chem* **1995**, *270*, 27695-27701, doi:10.1074/jbc.270.46.27695.

73.   Pei, J.; Grishin, N.V. Unexpected diversity in Shisa-like proteins suggests the importance of their roles as transmembrane adaptors. *Cell Signal* **2012**, *24*, 758-769, doi:10.1016/j.cellsig.2011.11.011.

74.   Albitar, M.; Peschle, C.; Liebhaber, S.A. Theta, zeta, and epsilon globin messenger RNAs are expressed in adults. *Blood* **1989**, *74*, 629-637 %@ 0006-4971, doi:10.1182/blood.V74.2.629.629.

75.   Shahbaz, S.; Xu, L.; Osman, M.; Sligl, W.; Shields, J.; Joyce, M.; Tyrrell, D.L.; Oyegbami, O.; Elahi, S. Erythroid precursors and progenitors suppress adaptive immunity and get invaded by SARS-CoV-2. *Stem Cell Reports* **2021**, *16*, 1165-1181, doi:10.1016/j.stemcr.2021.04.001.

76.   Huerga Encabo, H.; Grey, W.; Garcia-Albornoz, M.; Wood, H.; Ulferts, R.; Aramburu, I.V.; Kulasekararaj, A.G.; Mufti, G.; Papayannopoulos, V.; Beale, R.; et al. Human Erythroid Progenitors Are Directly Infected by SARS-CoV-2: Implications for Emerging Erythropoiesis in Severe COVID-19 Patients. *Stem Cell Reports* **2021**, *16*, 428-436, doi:10.1016/j.stemcr.2021.02.001.

77.   Kuleshov, M.V.; Stein, D.J.; Clarke, D.J.B.; Kropiwnicki, E.; Jagodnik, K.M.; Bartal, A.; Evangelista, J.E.; Hom, J.; Cheng, M.; Bailey, A.; et al. The COVID-19 Drug and Gene Set Library. *Patterns (N Y)* **2020**, *1*, 100090, doi:10.1016/j.patter.2020.100090.

78.   Xie, Z.; Bailey, A.; Kuleshov, M.V.; Clarke, D.J.B.; Evangelista, J.E.; Jenkins, S.L.; Lachmann, A.; Wojciechowicz, M.L.; Kropiwnicki, E.; Jagodnik, K.M.; et al. Gene Set Knowledge Discovery with Enrichr. *Curr Protoc* **2021**, *1*, e90, doi:10.1002/cpz1.90.

79.   Mazzitelli, I.; Bleichmar, L.; Ludueña, M.G.; Pisarevsky, A.; Labato, M.; Chiaradia, V.; Finocchieto, P.; Paulin, F.; Hormanstorfer, M.; Baretto, M.C.; et al. Immunoglobulin G Immune Complexes May Contribute to Neutrophil Activation in the Course of Severe Coronavirus Disease 2019. *J Infect Dis* **2021**, *224*, 575-585, doi:10.1093/infdis/jiab174.

80.   Dean, M.J.; Ochoa, J.B.; Sanchez-Pino, M.D.; Zabaleta, J.; Garai, J.; Del Valle, L.; Wyczechowska, D.; Baiamonte, L.B.; Philbrook, P.; Majumder, R.; et al. Severe COVID-19 Is Characterized by an Impaired Type I Interferon Response and Elevated Levels of

Arginase Producing Granulocytic Myeloid Derived Suppressor Cells. *Front Immunol* **2021**, *12*, 695972, doi:10.3389/fimmu.2021.695972.

81.   Meizlish, M.L.; Pine, A.B.; Bishai, J.D.; Goshua, G.; Nadelmann, E.R.; Simonov, M.; Chang, C.H.; Zhang, H.; Shallow, M.; Bahel, P.; et al. A neutrophil activation signature predicts critical illness and mortality in COVID-19. *Blood Adv* **2021**, *5*, 1164-1177, doi:10.1182/bloodadvances.2020003568.

82.   Wang, C.; Wang, S.; Li, D.; Chen, P.; Han, S.; Zhao, G.; Chen, Y.; Zhao, J.; Xiong, J.; Qiu, J.; et al. Human Cathelicidin Inhibits SARS-CoV-2 Infection: Killing Two Birds with One Stone. *ACS Infect Dis* **2021**, *7*, 1545-1554, doi:10.1021/acsinfecdis.1c00096.

83.   Lawrence, S.M.; Corriden, R.; Nizet, V. The Ontogeny of a Neutrophil: Mechanisms of Granulopoiesis and Homeostasis. *Microbiol Mol Biol Rev* **2018**, *82*, doi:10.1128/MMBR.00057-17.

84.   Fang, X.; Duan, S.F.; Gong, Y.Z.; Wang, F.; Chen, X.L. Identification of Key Genes Associated with Changes in the Host Response to Severe Burn Shock: A Bioinformatics Analysis with Data from the Gene Expression Omnibus (GEO) Database. *J Inflamm Res* **2020**, *13*, 1029-1041, doi:10.2147/JIR.S282722.

85.   Zeqiraj, E.; Sicheri, F. Getting a handle on glycogen synthase - Its interaction with glycogenin. *Mol Aspects Med* **2015**, *46*, 63-69, doi:10.1016/j.mam.2015.08.004.

86.   Theilgaard-Mönch, K.; Jacobsen, L.C.; Nielsen, M.J.; Rasmussen, T.; Udby, L.; Gharib, M.; Arkwright, P.D.; Gombart, A.F.; Calafat, J.; Moestrup, S.K.; et al. Haptoglobin is synthesized during granulocyte differentiation, stored in specific granules, and released by neutrophils in response to activation. *Blood* **2006**, *108*, 353-361, doi:10.1182/blood-2005-09-3890.

87.   Yağcı, S.; Serin, E.; Acicbe, Ö.; Zeren, M.; Odabaşı, M.S. The relationship between serum erythropoietin, hepcidin, and haptoglobin levels with disease severity and other biochemical values in patients with COVID-19. *Int J Lab Hematol* **2021**, *43 Suppl 1*, 142-151, doi:10.1111/ijlh.13479.

88.   Kumar, N.P.; Venkataraman, A.; Hanna, L.E.; Putlibai, S.; Karthick, M.; Rajamanikam, A.; Sadasivam, K.; Sundaram, B.; Babu, S. Systemic Inflammation and Microbial Translocation Are Characteristic Features of SARS-CoV-2-Related Multisystem Inflammatory Syndrome in Children. *Open Forum Infect Dis* **2021**, *8*, ofab279, doi:10.1093/ofid/ofab279.

89.   Yang, L.; Yang, Z.; Cheng, L.; Cheng, J.; Sun, Y.; Li, W.; Song, K.; Huang, W.; Yin, Y.; Tao, S.; et al. Lectin Microarray Combined with Mass Spectrometry Identifies Haptoglobin-Related Protein (HPR) as a Potential Serologic Biomarker for Separating Nonbacterial Pneumonia from Bacterial Pneumonia in Childhood. *Proteomics Clin Appl* **2018**, *12*, e1800030, doi:10.1002/prca.201800030.

90.   Barbut, D.; Stolzenberg, E.; Zasloff, M. Gastrointestinal Immunity and Alpha-Synuclein. *J Parkinsons Dis* **2019**, *9*, S313-S322, doi:10.3233/JPD-191702.

91.   Rosen, B.; Kurtishi, A.; Vazquez-Jimenez, G.R.; Møller, S.G. The Intersection of Parkinson's Disease, Viral Infections, and COVID-19. *Mol Neurobiol* **2021**, *58*, 4477-4486, doi:10.1007/s12035-021-02408-8.

92.   Miotto, M.; Di Rienzo, L.; Bò, L.; Boffi, A.; Ruocco, G.; Milanetti, E. Molecular Mechanisms Behind Anti SARS-CoV-2 Action of Lactoferrin. *Front Mol Biosci* **2021**, *8*, 607443, doi:10.3389/fmolb.2021.607443.

93.   Abers, M.S.; Delmonte, O.M.; Ricotta, E.E.; Fintzi, J.; Fink, D.L.; de Jesus, A.A.A.; Zarember, K.A.; Alehashemi, S.; Oikonomou, V.; Desai, J.V.; et al. An immune-based biomarker signature is associated with mortality in COVID-19 patients. *JCI Insight* **2021**, *6*, doi:10.1172/jci.insight.144455.

94.   Shrivastava, S.; Chelluboina, S.; Jedge, P.; Doke, P.; Palkar, S.; Mishra, A.C.; Arankalle, V.A. Elevated Levels of Neutrophil Activated Proteins, Alpha-Defensins (DEFA1), Calprotectin (S100A8/A9) and Myeloperoxidase (MPO) Are Associated With Disease Severity in COVID-19 Patients. *Front Cell Infect Microbiol* **2021**, *11*, 751232, doi:10.3389/fcimb.2021.751232.

95.   Zeng, Y.; Ma, W.; Ma, C.; Ren, X.; Wang, Y. Inhibition of TXNDC5 attenuates lipopolysaccharide-induced septic shock by altering inflammatory responses. *Lab Invest* **2021**, doi:10.1038/s41374-021-00711-5.

96.   Huang, D.; Liu, A.Y.N.; Leung, K.S.; Tang, N.L.S. Direct Measurement of B Lymphocyte Gene Expression Biomarkers in Peripheral Blood Transcriptomics Enables Early Prediction of Vaccine Seroconversion. *Genes (Basel)* **2021**, *12*, doi:10.3390/genes12070971.

97. Lopez-Castaneda, S.; García-Larragoiti, N.; Cano-Mendez, A.; Blancas-Ayala, K.; Damian-Vázquez, G.; Perez-Medina, A.I.; Chora-Hernández, L.D.; Arean-Martínez, C.; Viveros-Sandoval, M.E. Inflammatory and Prothrombotic Biomarkers Associated With the Severity of COVID-19 Infection. *Clin Appl Thromb Hemost* **2021**, *27*, 1076029621999099, doi:10.1177/1076029621999099.

98. Sai, K.; Kurose, K.; Koizumi, T.; Katori, N.; Sawada, J.; Matsumura, Y.; Saijo, N.; Yamamoto, N.; Tamura, T.; Okuda, H.; et al. Distal promoter regions are responsible for differential regulation of human orosomucoid-1 and -2 gene expression and acute phase responses. *Biol Pharm Bull* **2014**, *37*, 164-168, doi:10.1248/bpb.b13-00551.

99. Liu, X.; Cao, Y.; Fu, H.; Wei, J.; Chen, J.; Hu, J.; Liu, B. Proteomics Analysis of Serum from COVID-19 Patients. *ACS Omega* **2021**, *6*, 7951-7958, doi:10.1021/acsomega.1c00616.

100. Odle, R.I.; Florey, O.; Ktistakis, N.T.; Cook, S.J. CDK1, the Other 'Master Regulator' of Autophagy. *Trends Cell Biol* **2021**, *31*, 95-107, doi:10.1016/j.tcb.2020.11.001.

101. Auwul, M.R.; Rahman, M.R.; Gov, E.; Shahjaman, M.; Moni, M.A. Bioinformatics and machine learning approach identifies potential drug targets and pathways in COVID-19. *Brief Bioinform* **2021**, *22*, doi:10.1093/bib/bbab120.

102. Malumbres, M.; Barbacid, M. Mammalian cyclin-dependent kinases. *Trends Biochem Sci* **2005**, *30*, 630-641, doi:10.1016/j.tibs.2005.09.005.

103. Yu, M.; Xu, W.; Jie, Y.; Pang, J.; Huang, S.; Cao, J.; Gong, J.; Li, X.; Chong, Y. Identification and validation of three core genes in p53 signaling pathway in hepatitis B virus-related hepatocellular carcinoma. *World J Surg Oncol* **2021**, *19*, 66, doi:10.1186/s12957-021-02174-w.

104. Chen, J.C.; Xie, T.A.; Lin, Z.Z.; Li, Y.Q.; Xie, Y.F.; Li, Z.W.; Guo, X.G. Identification of Key Pathways and Genes in SARS-CoV-2 Infecting Human Intestines by Bioinformatics Analysis. *Biochem Genet* **2021**, doi:10.1007/s10528-021-10144-w.

105. Gravina, G.; Wasén, C.; Garcia-Bonete, M.J.; Turkkila, M.; Erlandsson, M.C.; Töyrä Silfverswärd, S.; Brisslert, M.; Pullerits, R.; Andersson, K.M.; Katona, G.; et al. Survivin in autoimmune diseases. *Autoimmun Rev* **2017**, *16*, 845-855, doi:10.1016/j.autrev.2017.05.016.

106. Pulkkinen, H.H.; Kiema, M.; Lappalainen, J.P.; Toropainen, A.; Beter, M.; Tirronen, A.; Holappa, L.; Niskanen, H.; Kaikkonen, M.U.; Ylä-Herttuala, S.; et al. BMP6/TAZ-Hippo signaling modulates angiogenesis and endothelial cell response to VEGF. *Angiogenesis* **2021**, *24*, 129-144, doi:10.1007/s10456-020-09748-4.

107. Jiang, P.; Zhang, Y.; Ru, B.; Yang, Y.; Vu, T.; Paul, R.; Mirza, A.; Altan-Bonnet, G.; Liu, L.; Ruppin, E.; et al. Systematic investigation of cytokine signaling activity at the tissue and single-cell levels. *Nat Methods* **2021**, *18*, 1181-1191, doi:10.1038/s41592-021-01274-5.

108. Liu, J.; Cao, S.; Ding, G.; Wang, B.; Li, Y.; Zhao, Y.; Shao, Q.; Feng, J.; Liu, S.; Qin, L.; et al. The role of 14-3-3 proteins in cell signalling pathways and virus infection. *J Cell Mol Med* **2021**, *25*, 4173-4182, doi:10.1111/jcmm.16490.

109. Laforge, M.; Elbim, C.; Frère, C.; Hémadi, M.; Massaad, C.; Nuss, P.; Benoliel, J.J.; Becker, C. Tissue damage from neutrophil-induced oxidative stress in COVID-19. *Nat Rev Immunol* **2020**, *20*, 515-516, doi:10.1038/s41577-020-0407-1.

110. Girkin, J.L.N.; Maltby, S.; Bartlett, N.W. Toll-like receptor-agonist-based therapies for respiratory viral diseases: thinking outside the cell. *Eur Respir Rev* **2022**, *31*, doi:10.1183/16000617.0274-2021.

111. Ramasamy, R. Innate and Adaptive Immune Responses in the Upper Respiratory Tract and the Infectivity of SARS-CoV-2. *Viruses* **2022**, *14*, doi:10.3390/v14050933.

112. Wylezich, C.; Schaller, T.; Claus, R.; Hirschbühl, K.; Märkl, B.; Kling, E.; Spring, O.; Höper, D.; Schlegel, J.; Beer, M.; et al. Whole-genome analysis of SARS-CoV-2 samples indicate no tissue specific genetic adaptation of the virus in COVID-19 patients' upper and lower respiratory tract. *Diagn Microbiol Infect Dis* **2021**, *101*, 115520, doi:10.1016/j.diagmicrobio.2021.115520.

113. Dhochak, N.; Singhal, T.; Kabra, S.K.; Lodha, R. Pathophysiology of COVID-19: Why Children Fare Better than Adults? *Indian J Pediatr* **2020**, *87*, 537-546, doi:10.1007/s12098-020-03322-y.

114. Burkert, F.R.; Lanser, L.; Bellmann-Weiler, R.; Weiss, G. Coronavirus Disease 2019: Clinics, Treatment, and Prevention. *Front Microbiol* **2021**, *12*, 761887, doi:10.3389/fmicb.2021.761887.

115.   Statsenko, Y.; Al Zahmi, F.; Habuza, T.; Almansoori, T.M.; Smetanina, D.; Simiyu, G.L.; Neidl-Van Gorkom, K.; Ljubisavljevic, M.; Awawdeh, R.; Elshekhali, H.; et al. Impact of Age and Sex on COVID-19 Severity Assessed From Radiologic and Clinical Findings. *Front Cell Infect Microbiol* **2022**, *11*, 777070, doi:10.3389/fcimb.2021.777070.